J. Fluid Mech. (1997), *vol.* 333, *pp.* 197–230

Dynamics of vorticity defects in shear

By N. J. BALMFORTH[1], D. DEL-CASTILLO-NEGRETE[2] AND W. R. YOUNG[2]

[1]Department of Theoretical Mechanics, University of Nottingham, Nottingham, NG7 2RD, UK
[2]Scripps Institution of Oceanography, University of California at San Diego, La Jolla, CA 92093-0230, USA

(Received 10 May 1996 and in revised form 11 September 1996)

Matched asymptotic expansions are used to obtain a reduced description of the nonlinear and viscous evolution of small, localized vorticity defects embedded in a Couette flow. This vorticity defect approximation is similar to the Vlasov equation, and to other reduced descriptions used to study forced Rossby wave critical layers and their secondary instabilities. The linear stability theory of the vorticity defect approximation is developed in a concise and complete form. The dispersion relations for the normal modes of both inviscid and viscous defects are obtained explicitly. The Nyquist method is used to obtain necessary and sufficient conditions for instability, and to understand qualitatively how changes in the basic state alter the stability properties. The linear initial value problem is solved explicitly with Laplace transforms; the resulting solutions exhibit the transient growth and eventual decay of the streamfunction associated with the continuous spectrum. The expansion scheme can be generalized to handle vorticity defects in non-Couette, but monotonic, velocity profiles.

1. Introduction

One of the most challenging problems in fluid dynamics is the evolution of disturbances on a shear flow at very high Reynolds number. Such situations arise in laboratory and industrial settings, as well as in the fluid envelopes of planets, in stars and in circumstellar disks. It is common to attack shear flow problems of this kind by either idealizing the fluid as inviscid, or including the small viscosity as a perturbation. It is from this direction that much of the complication arises: the mathematics of ideal fluids entails difficulties such as critical layer singularities, continuous spectra and continuum damping (and amplification) produced by phase mixing. The introduction of small viscosity has all the attendant difficulties of singular perturbation problems.

The main thrust of this paper is to study the dynamics of a particular kind of shear flow. Specifically, we consider a shearing flow in which there is embedded a localized region over which the vorticity varies rapidly. That is, a situation in which there is some strong, ambient shear, but seeded within it is a rapidly varying 'defect', like that shown in figure 1. One can use a matched asymptotic expansion to produce a simplified description of the evolution of this *vorticity defect*. Linear and inviscid versions of this approximation have been developed by Gill (1965) and Lerner & Knobloch (1988). These authors consider defects of inviscid Couette flow; they show that this slight imperfection can be sufficient to destabilize the shear flow.

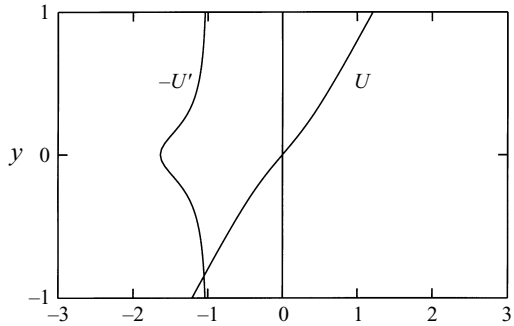

FIGURE 1. An illustration of the shear flow configuration under discussion in this paper. The velocity profile, $U(y)$, is largely a two-dimensional and incompressible Couette flow, with a superposed *vorticity defect*.

However, these earlier works do not fully exploit the simplifications which follow from the assumption of a localized vorticity defect. We continue to mine this vein by showing that both dissipative effects and advective nonlinearity can be included in the approximation. Hence, the approximation enables us to present a rather complete picture of linear stability theory (both ideal and viscous), and to advance into the nonlinear regime with substantially less effort than if we were to follow the usual route from the Navier–Stokes equations.

The matched asymptotic expansion that we use in §3 is similar to, though simpler than, the method used by Stewartson (1978), Warn & Warn (1978), Killworth & McIntyre (1985) and Haynes (1985, 1987, 1989) in the study of forced Rossby wave critical layers and their instabilities. The Rossby wave critical layer problem is not primarily a hydrodynamic stability problem because a wave-like disturbance is forced by the passage of a shear flow over a corrugated boundary: in this case the connection between frequency and wavenumber is imposed externally by the spacing of the corrugations and the speed of the shear flow. By contrast, we are concerned here with the possibly spontaneous growth of wave-like disturbances whose linear dispersion relation is not known in advance. The waves we consider in this paper do have critical layers, but these regions are asymptotically embedded within the vorticity defect.

The most unappealing feature of the approximation is that, because attention is restricted to disturbances localized within the defect, there is no guarantee that the asymptotic formulation captures the dominant processes occurring over the entire shear flow. But the approximation does allow us to elucidate some physical processes very readily. For purely inviscid disturbances, we are led to an approximate description that bears some similarity to the Vlasov equation of plasma physics. Although the Vlasov equation is more tractable than the original Euler equation it does describe strongly nonlinear processes such as the formation of coherent structures and the development of subcritical instabilities.

The main results that we give in this paper are directed towards the derivation of the equations of motion for the vorticity defect and the construction of a complete linear stability theory for disturbances within it. For the sake of simplicity, we develop the theory for a plane parallel, background shear flow which is linear; that is, an ambient Couette flow like that shown in figure 1. This simplification is not essential, and in an Appendix we develop a more general theory. A preliminary study of the nonlinear regime is given by del-Castillo-Negrete, Young & Balmforth (1995).

Sections 2 and 3 are concerned with the derivation of the approximate equations of motion. In §4 we turn to a discussion of the conservation laws for energy, momentum and circulation which the approximate system inherits from the Navier–Stokes equation. In §5 we begin our discussion of the linear stability of parallel flows by solving the inviscid normal-mode stability problem (the analog of the Rayleigh equation) for some specific basic states. In §6 we present a Nyquist method which provides necessary and sufficient conditions for determining the stability of an arbitrary basic state. Section 7 deals with inviscid initial-value problems, and §8 develops the linear stability theory for viscous flows. Section 9 is the conclusion and discussion. The appendix develops a more general version of the approximation which includes the β-effect (the gradient of the planetary rotation rate) and non-uniform background shear.

2. Formulation of the problem

Our point of departure is the forced two-dimensional vorticity equation,

$$\hat{\nabla}^2\hat{\Psi}_{\hat{t}} + \frac{\partial(\hat{\Psi}, \hat{\nabla}^2\hat{\Psi})}{\partial(\hat{x}, \hat{y})} = \hat{\alpha}\left(\hat{\zeta}_F - \hat{\nabla}^2\hat{\Psi}\right) - \hat{\nu}\hat{\nabla}^2\left(\hat{\zeta}_F - \hat{\nabla}^2\hat{\Psi}\right). \tag{2.1}$$

The domain is $-\hat{b} < \hat{y} < \hat{b}$ and $-\infty < \hat{x} < \infty$, the velocity is $(\hat{u}, \hat{v}) = (-\hat{\Psi}_{\hat{y}}, \hat{\Psi}_{\hat{x}})$, and the vorticity is $\hat{v}_{\hat{x}} - \hat{u}_{\hat{y}} = \hat{\nabla}^2\hat{\Psi}$. The right-hand side of (2.1) includes damping by both Ekman friction with a time scale $\hat{\alpha}^{-1}$, and momentum diffusion with a coefficient of kinematic viscosity $\hat{\nu}$. Motion is sustained by forcing, $\hat{\zeta}_F(\hat{x}, \hat{y})$. As boundary conditions on (2.1), we impose

$$\hat{\Psi}(\hat{x}, \pm\hat{b}, \hat{t}) = 0, \qquad \hat{\Psi}_{\hat{y}}(\hat{x}, \pm\hat{b}, \hat{t}) = \mp s\hat{b}, \qquad \hat{\Psi}(\hat{x}, \hat{y}, \hat{t}) = \hat{\Psi}(\hat{x} + \hat{a}, \hat{y}, \hat{t}). \tag{2.2a,b,c}$$

The central assumption made in this paper is that $\hat{\zeta}_F$, the equilibrium vorticity distribution towards which forcing and dissipation equilibrate, has the form

$$\hat{\zeta}_F = -s + \epsilon s F\left(y/\epsilon\right), \tag{2.3}$$

where ϵ is a small non-dimensional parameter, s is a constant with the dimensions of inverse time, and where the dimensionless coordinates are

$$(x, y) \equiv \hat{b}^{-1}(\hat{x}, \hat{y}). \tag{2.4}$$

The dimensionless function F in (2.3) is assumed to decay quickly when the argument y/ϵ is large; in fact, we insist that $F \lesssim (y/\epsilon)^{-2}$. The parameter, ϵ, controls the localization of the 'vorticity defect,' F, relative to the width of the channel. If $F = 0$ then the forcing drives a pure Couette flow with $\hat{u} = s\hat{y}$ and $\hat{v} = 0$. More general configurations are discussed in the Appendix.

We now non-dimensionalize (2.1) by setting

$$\hat{\Psi}(\hat{x}, \hat{y}, \hat{t}) = -\tfrac{1}{2}sb^2\left(y^2 - 1\right) + \epsilon^2 sb^2\psi(x, y, t), \tag{2.5}$$

and defining the following non-dimensional variables:

$$t = \epsilon s\hat{t}, \qquad \nu = \hat{\nu}/(\epsilon^3 sb^2), \qquad \alpha = \hat{\alpha}/(\epsilon s). \tag{2.6a,b,c}$$

We refer to $\psi(x, y, t)$ as the 'disturbance', meaning that this field contains all departures from the Couette flow.

The non-dimensional equation of motion for the disturbance is then

$$\epsilon\nabla^2\psi_t + y\nabla^2\psi_x + \epsilon^2\frac{\partial(\psi,\nabla^2\psi)}{\partial(x,y)} = \epsilon\alpha\left(\epsilon^{-1}F - \nabla^2\psi\right) - \epsilon^3\nu\nabla^2\left(\epsilon^{-1}F - \nabla^2\psi\right). \tag{2.7}$$

Equation (2.7) is scaled in the most convenient form for the 'outer' expansion, that is, the solution in the regions where $y/\epsilon \gg 1$.

3. The vorticity defect approximation

In this section we develop the 'vorticity defect approximation' using a matched asymptotic expansion of (2.7).

3.1. *The outer solution*

In the outer region, where $y = O(1)$, we assume that the forcing function, F, is small. In this case (2.7) can be solved with an expansion,

$$\psi = \psi_0 + \epsilon\psi_1 + \cdots. \tag{3.1}$$

The leading-order balance in (2.7) is

$$y\nabla^2\psi_0 = 0, \tag{3.2}$$

so that the disturbance motion in the outer region is irrotational at leading order. On dividing out the factor y in (3.2), we find

$$\nabla^2\psi_0 = -2A(x,t)\delta(y), \tag{3.3}$$

where $A(x,t)$ is an undetermined function allowing for what appears to be a vortex sheet at the defect. The physical interpretation of (3.3) is that all of the disturbance vorticity is confined to the defect where $y = O(\epsilon)$. To the flow in the outer field this vorticity concentration looks like a δ-function with an evolving strength, $A(x,t)$. This δ-function singularity produces a jump in the leading order x-velocity at $y = 0$,

$$\psi_{0y}(x,0^+,t) - \psi_{0y}(x,0^-,t) = -2A(x,t). \tag{3.4}$$

The discontinuity in the outer velocity is smoothed on the scale ϵ by the inner expansion.

The streamfunction can be obtained from (3.3) using a Fourier transform,

$$\tilde{\psi}_0(k,y,t) \equiv \int_{-\infty}^{\infty}\psi_0(x,y,t)\mathrm{e}^{-\mathrm{i}kx}\,\mathrm{d}x. \tag{3.5}$$

In terms of the transformed streamfunction, equation (3.3) is

$$\tilde{\psi}_{0yy} - k^2\tilde{\psi}_0 = -2\tilde{A}\delta(y). \tag{3.6}$$

For the purpose of matching with the inner solution it is convenient to introduce

$$B(x,t) \equiv \psi_0(x,0,t), \tag{3.7}$$

and write the solution of (3.6), with boundary conditions $\tilde{\psi}(k,\pm1,t) = 0$, as

$$\tilde{\psi}_0(k,y,t) = \tilde{A}(k,t)k^{-1}\mathrm{sech}(k)\sinh\left[k(1-|y|)\right] \tag{3.8a}$$

$$= \tilde{B}(k,t)\mathrm{cosech}(k)\sinh\left[k(1-|y|)\right] \tag{3.8b}$$

$$= \tilde{B} - \tilde{A}|y| + O(y^2). \tag{3.8c}$$

In (3.8*c*) we have indicated the $|y| \ll 1$ expansion of the streamfunction: the velocity jump in (3.4) is evident. From (3.8*a*) and (3.8*b*) it follows that

$$\tilde{B}(k,t) = k^{-1}\tanh(k)\tilde{A}(k,t), \qquad B(x,t) = \int_{-\infty}^{\infty} \mathscr{K}(x-x')A(x',t)\,\mathrm{d}x', \tag{3.9a,b}$$

where $\mathscr{K}(x) = \pi^{-1}\ln\left[|\coth(\pi x/4)|\right]$ is the inverse Fourier transform of $\tilde{\mathscr{K}}(k) \equiv k^{-1}\tanh k$.

We summarize the calculation above by saying that the outer flow is driven by the defect, which introduces the term $-2A(x,t)\delta(y)$ into the right-hand side of (3.3). This source induces an irrotational outer flow which in turn advects the defect. This advection is associated with the streamfunction at the defect, denoted by $B(x,t)$ in (3.7). The two fields A and B are connected by (3.9). The system is closed by examining the inner region in which $y = O(\epsilon)$.

3.2. *The inner region*

Inside the defect we define an inner variable,

$$\eta \equiv \frac{y}{\epsilon}. \tag{3.10}$$

We simplify (2.7) by posing a solution of the form

$$\psi = B(x,t) + \epsilon\varphi_1(x,\eta,t) + O(\epsilon^2), \tag{3.11a}$$

$$\psi_y = \varphi_{1\eta} + \epsilon\varphi_{2\eta} + O(\epsilon^2), \tag{3.11b}$$

$$\nabla^2\psi = \epsilon^{-1}\varphi_{1\eta\eta} + B_{xx} + \varphi_{2\eta\eta} + O(\epsilon). \tag{3.11c}$$

The function $B(x,t)$ on the right-hand side of (3.11*a*) is the value of the outer streamfunction at $y = 0$. Thus a match between the outer solution in (3.8) and the inner solution in (3.11*a*) is secured. The outer solution in (3.8) also has a jump in its y-derivative at $y = 0$. In physical space this discontinuity of size $2A(x,t)$ is smoothed by the inner solution in (3.11). Thus the second matching condition is

$$2A(x,t) = -\int_{-\infty}^{\infty} Z(x,\eta,t)\,\mathrm{d}\eta, \tag{3.12}$$

where the leading-order vorticity in (3.11*c*) is

$$Z(x,\eta,t) \equiv \varphi_{1\eta\eta}. \tag{3.13}$$

The velocity jump across the defect is equal to the integrated vorticity within the defect.

The evolution equation for $Z(x,\eta,t)$ is now obtained by substituting (3.11) into (2.7) and collecting the leading-order terms. One finds that the difficult nonlinear term, $\partial(\varphi_1, \varphi_{1\eta\eta})/\partial(x,\eta)$, is smaller by $O(\epsilon)$ than the leading-order contributions.

We can collect the results of the inner and the outer expansions and form the vorticity defect equation:

$$Z_t + \eta Z_x + B_x Z_\eta = \alpha(F - Z) - \nu(F - Z)_{\eta\eta}, \tag{3.14a}$$

$$2\tilde{B}(k,t) = -k^{-1}\tanh k \int_{-\infty}^{\infty} \tilde{Z}(k,\eta,t)\,\mathrm{d}\eta. \tag{3.14b}$$

The remainder of this paper is concerned with the solution of (3.14).

An important feature of the vorticity defect approximation in (3.14) is that, when we set the dissipative terms to zero, it becomes analogous to the Vlasov equation of

plasma physics (e.g. Nicholson 1983). In this analogy, η is a velocity-like coordinate, the defect vorticity, $Z(x,\eta,t)$, plays the role of particle distribution function, and $B(x,t)$ corresponds to the potential of the electric field. The two problems differ in that, whereas the particle distribution function is always positive for the Vlasov problem, the vorticity in (3.14*a*) can have either sign, and in that the relation in (3.14*b*) is more complicated than the Poisson equation which occurs in the Vlasov case.

4. Conservation laws

In this section we show that the vorticity defect approximation in (3.14) inherits all of the conservation laws of the complete equations of motion. In view of our interest in conserved quantities we restrict attention to the unforced and dissipationless version of (3.14*a*, *b*), i.e. we now take $\alpha = \nu = 0$. Because (3.14*a*) is an advection equation, with a streamfunction, $B-\eta^2/2$, there is an infinitude of vorticity invariants corresponding to rearrangements of Z. That is to say

$$\frac{\mathrm{d}}{\mathrm{d}t}\int_{-\infty}^{\infty}\int_{-\infty}^{\infty}\mathscr{C}(Z)\,\mathrm{d}\eta\mathrm{d}x = 0, \tag{4.1}$$

where $\mathscr{C}$ is any function.

Additionally, there is a momentum invariant,

$$\frac{\mathrm{d}}{\mathrm{d}t}\int_{-\infty}^{\infty}\int_{-\infty}^{\infty}\eta Z\,\mathrm{d}\eta\mathrm{d}x = 0, \tag{4.2}$$

and an energy invariant,

$$\frac{\mathrm{d}}{\mathrm{d}t}\left[\frac{1}{2}\int_{-\infty}^{\infty}\int_{-\infty}^{\infty}\eta^2 Z\,\mathrm{d}\eta\mathrm{d}x + \int_{-\infty}^{\infty}AB\,\mathrm{d}x\right] = 0. \tag{4.3}$$

The energy in (4.3) is divided between the outer irrotational field, $\int AB\,\mathrm{d}x$, and the inner vortical field, $\int\int(\eta^2 Z/2)\mathrm{d}x\mathrm{d}\eta$. The conservation laws in (4.1) follow from (3.14*a*) alone, whereas to obtain (4.2) and (4.3) one must also use the relation in (3.14*b*).

5. Inviscid linear stability theory for some specific profiles

Our primary goal in this section is to use the vorticity defect approximation in (3.14) to solve the linear stability problem for some specific vorticity profiles. The analogous linearized stability problem for the full equations of motion is the Rayleigh equation (Drazin & Howard 1966; Maslowe 1985). Setting aside 'broken-line' profiles, there are only a few explicit solutions of the Rayleigh equation available, and these are usually restricted to isolated regular neutral modes which mark stability boundaries. Even though the broken-line idealization leads to straightforward calculations, the ensuing artificial elimination of critical layer singularities means that the results so obtained are not compelling if one is interested in smooth profiles (Maslowe 1985). As we now illustrate, the defect approximation results in comparably simple calculations which capture the important effects of critical layer singularities.

5.1. *The inviscid dispersion relation and the Rayleigh–Fjørtoft theorem*

One class of steady solutions of (3.14) are parallel flows in which Z and B are independent of x. We study the linear stability of these parallel flows by substituting

$$Z(x,\eta,t) = F(\eta) + \zeta(x,y,t), \tag{5.1a}$$

$$B(x,t) = \frac{1}{2}\int_{-\infty}^{\infty}F(\eta')\,\mathrm{d}\eta' + b(x,t), \tag{5.1b}$$

into (3.14) and neglecting both the nonlinear term, $b_x\zeta_y$, and the dissipative effects ($\nu = \alpha = 0$). Thus, the associated linear problem of (3.14) is

$$\zeta_t + \eta\zeta_x + b_x F_\eta = 0, \tag{5.2a}$$

$$2\tilde{b}(k,t) = -k^{-1}\tanh k \int_{-\infty}^{\infty} \tilde{\zeta}(k,\eta,t)\,\mathrm{d}\eta. \tag{5.2b}$$

In §7 we discuss the solution of (5.2) as an initial value problem and in §8 we include the effects of dissipation. In this section we address the problem of finding modal solutions of (5.2). This means that we look for solutions of the form $\zeta(x,\eta,t) = \mathscr{Z}(\eta)\exp(\mathrm{i}kx - \mathrm{i}\omega t)$. On substituting this modal form into (5.2), we obtain the eigenfunction,

$$\mathscr{Z}(\eta) = \tfrac{1}{2}k^{-1}\tanh k\,\frac{F_\eta(\eta)}{\eta - c}\int_{-\infty}^{\infty}\mathscr{Z}(\eta_1)\,\mathrm{d}\eta_1, \tag{5.3}$$

where the phase speed is $c = \omega/k = c_r + \mathrm{i}c_i$. By integrating (5.3) over η we recover Gill's (1965) dispersion relation,

$$\int_{-\infty}^{\infty}\frac{F_\eta(\eta)}{\eta - c}\,\mathrm{d}\eta = 2k\coth k. \tag{5.4}$$

The ease with which we have obtained the dispersion relation in (5.4) illustrates the advantages of the vorticity defect approximation over the Rayleigh equation. In the next subsection we will evaluate the integral in (5.4) for some specific vorticity defect profiles.

To conclude this subsection we record the analogues of the Rayleigh and Fjørtoft stability theorems. These are obtained by separating the real and imaginary parts of (5.4):

$$\int_{-\infty}^{\infty}\frac{F_\eta(\eta)(\eta - c_r)}{(\eta - c_r)^2 + c_i^2}\,\mathrm{d}\eta = 2k\coth k, \tag{5.5a}$$

$$\int_{-\infty}^{\infty}\frac{c_i F_\eta(\eta)}{(\eta - c_r)^2 + c_i^2}\,\mathrm{d}\eta = 0. \tag{5.5b}$$

It follows immediately from (5.5*b*) that, if $c_i \neq 0$, then $F_\eta(\eta)$ must change sign at least once. This is Rayleigh's necessary condition for the existence of an unstable eigenmode. In the present context this result is nugatory because all defect vorticity profiles will have at least one point where $F_\eta = 0$.

To obtain the Fjørtoft theorem, we suppose that $c_i \neq 0$ and that there is a point, η_*, at which

$$F_\eta(\eta_*) = 0 \tag{5.6}$$

(that is, an inflection point of the velocity profile). If we take a linear combination of (5.5*a*) and (5.5*b*), then we obtain

$$c_i \neq 0 \quad \Rightarrow \quad \int_{-\infty}^{\infty}\frac{F_\eta(\eta)(\eta - \eta_*)}{(\eta - \eta_*)^2 + c_i^2}\,\mathrm{d}\eta = 2k\coth k. \tag{5.7}$$

In certain cases it is possible to prove that (5.7) leads to a contradiction so that the profile is stable even though there is an inflection point at η_*. For example, if there is only a single inflection point then the function $F_\eta(\eta)(\eta - \eta_*)$ has a definite sign, which is the same as the sign of $F_{\eta\eta}(\eta_*)$. Thus profiles with a single inflection point, η_*, and $F_{\eta\eta}(\eta_*) < 0$ are stable because in this case the integral on the left-hand side of (5.7) is negative, whereas the right-hand side is positive.

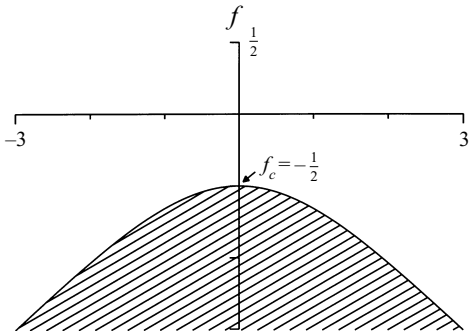

FIGURE 2. The region of the (k, f)-plane in which the top-hat vorticity profile has an unstable mode is shaded. If $f > -1/2$ the profile is stable.

As an illustration, consider a basic state with a 'Lorentzian' vorticity profile:

$$F(\eta) = \frac{f}{1+\eta^2}. \tag{5.8}$$

This profile is stable when $f > 0$ (i.e. $F_{\eta\eta}(\eta_*) < 0$) even though it has a velocity inflection point at $\eta_* = 0$. But $f < 0$ (i.e. $F_{\eta\eta}(\eta_*) > 0$) is not sufficient for instability; in §5.3 we show by explicit solution that linear instability occurs only if $f < -2/\pi$. Thus, as usual, the Fjørtoft condition is necessary, but not sufficient, for instability. In §6, we improve on this situation by describing a Nyquist method that leads to necessary *and* sufficient conditions for instability.

5.2. *The top-hat profile*

We begin with a simple special case by selecting a 'top-hat' profile for $F(\eta)$:

$$F(\eta) = \begin{cases} f & \text{if } |\eta| < \frac{1}{2} \\ 0 & \text{if } |\eta| > \frac{1}{2}. \end{cases} \tag{5.9a}$$

The vorticity profile in (5.9) is equivalent to a broken-line velocity profile. In this case,

$$F_\eta(\eta) = f\left[\delta\left(\eta + \tfrac{1}{2}\right) - \delta\left(\eta - \tfrac{1}{2}\right)\right]. \tag{5.9b}$$

Because of the δ-functions, the integral in (5.4) is trivial and one finds the dispersion relation

$$c^2 = \tfrac{1}{4} + \tfrac{1}{2} f k^{-1} \tanh(k). \tag{5.10a}$$

If $f < -k\coth k/2$, this relation has the complex conjugate solutions

$$c = \pm \mathrm{i}\left[\frac{|f|}{2k}\tanh k - \tfrac{1}{4}\right]^{1/2}; \tag{5.10b}$$

that is, a growing/decaying conjugate pair of modes. If, on the other hand, $f > -k\coth k/2$, the dispersion relation has a pair of real solutions, or two neutral modes. The relation $f = -k\coth k/2$ is therefore the stability boundary, which is illustrated in the (k, f)-plane in figure 2. The shaded region below the curve contains the instability; in the unshaded region above the curve, there are the two neutral modes. The bifurcation to instability occurs when the two neutral modes collide at the origin of the complex c-plane, then move off the real axis as the complex conjugate pair in (5.10*b*). This is an example of the Hamiltonian Hopf bifurcation (for each

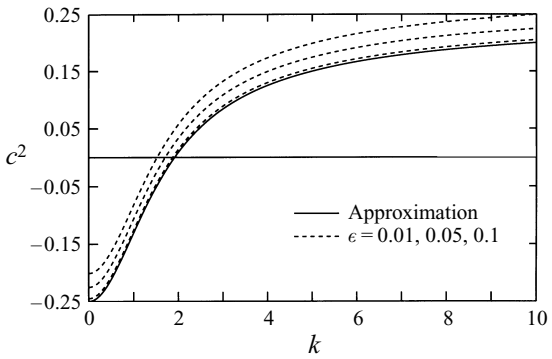

FIGURE 3. A comparison of the approximate dispersion relation in (5.10) with the exact result obtained from the Rayleigh equation. $f = -1$.

colliding pair with $k > 0$, there is a complementary duo with $k < 0$, so this is the usual interaction of a modal quartet).

In figure 3 we compare (5.10) with the exact result that is available from Rayleigh's equation (e.g. Drazin & Howard 1966). One remarkable aspect of this comparison is that the exact and approximate curves parallel each other with an offset which remains constant as k increases. The offset in figure 3 is proportional to ϵ in (2.3), so that the curves coincide as $\epsilon \to 0$. A surprising point is that the approximation is accurate even when $k = O(\epsilon^{-1})$. Thus the approximation does not seriously misrepresent the linear dynamics of small-scale disturbances whose inverse wavenumber is comparable to the width of the defect. Unfortunately, as illustrated by the Lorentzian example below, this accuracy is a peculiarity of the top-hat vorticity profile.

5.3. *The Lorentzian profile*

The normal modes of the top-hat vorticity profile do not possess critical layer singularities: the integral in the dispersion relation (5.4) is non-singular even when c is real (except in the pathological case when the critical layer lines up along one of the vorticity discontinuities). Consequently the top-hat profile has a pair of discrete neutral modes, with $c_i = 0$, in the unshaded portion of the (k, f)-plane in figure 2.

As an example of a less trivial basic state, we consider the Lorentzian profile of (5.8). Provided that c has a non-zero imaginary part, the integral in the dispersion relation (5.4) is non-singular and can be evaluated with the Cauchy residue theorem. The result is

$$\frac{f\pi}{2k}\tanh k = \begin{cases} (c+\mathrm{i})^2 & \text{if } c_\mathrm{i} > 0 \\ (c-\mathrm{i})^2 & \text{if } c_\mathrm{i} < 0. \end{cases} \tag{5.11}$$

In order for the relation (5.11) to be consistent, we require

$$\frac{\pi f}{2k}\tanh k < -1. \tag{5.12}$$

In that case, we find

$$c = \pm\mathrm{i}\left(\left[\frac{\pi|f|}{2k}\tanh k\right]^{1/2} - 1\right), \tag{5.13}$$

which, as for the broken-line profile, reveals a growing/decaying mode pair.

The stability boundary is given by the relation $f = -2k\coth k/\pi$. We illustrate this boundary on the (k, f)-plane in figure 4; the conjugate pair of modes with $c_i \neq 0$ in

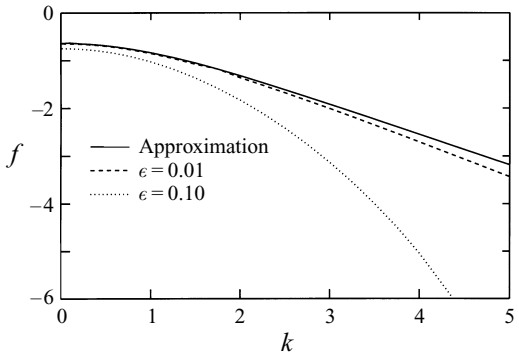

FIGURE 4. The stability boundary in the (k, f)-plane for the Lorentzian (the region below the curve is unstable). Also shown is the stability boundary obtained from a numerical calculation of the eigenmodes of the Lorentzian vorticity profile using the full Rayleigh equation. Two curves are shown representing calculations in which $\epsilon = 0.1$ and $\epsilon = 0.01$. The error in the defect approximation is of the order of ϵk^2. Thus the approximation fails both for defects which are either not sufficiently localized in η, or for perturbations that vary rapidly in x.

(5.13) exists in the region below the solid curve. This region is qualitatively similar to the unstable region of the top hat shown in figure 2. Both cases have similarly shaped stability boundaries with marginal stability points at $k = 0$; for the Lorentzian, the marginally stable profile is given by $f_c = -2/\pi$.

In contrast to the top hat, however, if the parameters do not satisfy (5.12), then there is no consistent solution to the dispersion relation, (5.11). In other words, it is *not* the case that we can construct neutral modes with $c_i = 0$, in the region above the solid curve in figure 4. In fact, if $c_i = 0$, there is an unphysical singularity in the linear eigenmode, (5.3), at the critical layer, unless this layer coincides with an inflection point. We conclude that for the stable case the linear problem in (5.2) does not have, in general, smooth solutions proportional to $\exp(\mathrm{i}kx - \mathrm{i}\omega t)$. This signifies the existence of the continuous spectrum of singular eigenmodes in which there is no definite connection between the wavenumber and frequency of a disturbance. Thus the bifurcation to instability in (5.13) is an example of a Hamiltonian Hopf bifurcation in which a complex conjugate pair of modes emerges from a continuous spectrum.

5.4. *Finite-wavelength instabilities*

In both of the examples above, the instability is confined to long wavelength so that the critical wavenumber is $k_c = 0$. It is interesting to consider basic states with more structure so that there is a shear flow instability with a finite critical wavenumber. To this end we consider a family of vorticity profiles with three parameters,

$$F(\eta) = f\frac{1 + p\eta + q\eta^2}{(1+\eta^2)^2}. \tag{5.14}$$

The 'shape parameters' p and q can be adjusted to produce a vorticity profile with as many as three extrema (see figure 5). As before, the parameter f controls the overall magnitude of the vorticity bump.

If $c_i \neq 0$, then a residue evaluation of the integral in the dispersion relation (5.4) gives

$$k\coth k = \frac{\pi}{4} f\left[\frac{1+q}{(\mathrm{i}+c)^2} + 2\frac{p+(1-q)\mathrm{i}}{(\mathrm{i}+c)^3}\right] \quad \text{if} \quad c_i > 0. \tag{5.15}$$

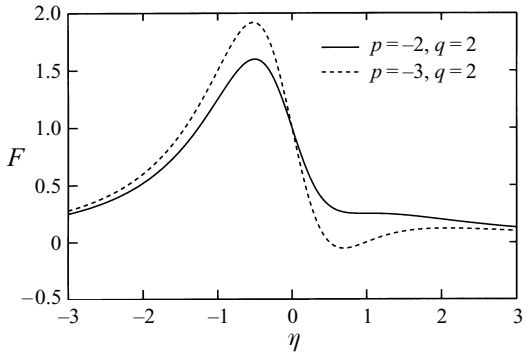

FIGURE 5. Two vorticity profiles from the family in (5.14).

Equation (5.15) reduces to (5.11) when $(p, q) = (0, 1)$ and so we anticipate that if f is sufficiently negative we will once again find a long-wavelength instability. In view of our interest in instabilities with finite k_c we restrict attention to $f > 0$ and focus on the particular family of profiles with $q = 2$ (illustrated in figure 5). When $p = -2$, the defect profile has a double inflection point at $\eta = 1$. That is, $F'(1) = F''(1) = 0$. We anticipate that this flow is marginally stable since profiles with smaller values of p contain two inflection points straddling $\eta = 1$.

We now rewrite (5.15), with $q = 2$, as a cubic polynomial in c:

$$c^3 + 3\mathrm{i}c^2 - \tfrac{3}{2}(2+\rho)c - \rho p - \tfrac{1}{2}(2+\rho)\mathrm{i} = 0 \quad \text{if} \quad c_\mathrm{i} > 0. \tag{5.16}$$

In (5.16) we have introduced the parameter,

$$\rho \equiv \frac{\pi f}{2k}\tanh k. \tag{5.17}$$

The stability boundary in the three-dimensional space (k, f, p) is located by assuming that $c_i = 0$ and separating the real and imaginary parts in (5.16). In this way we find that on the stability boundary

$$c^2 = \frac{2+\rho}{6}, \qquad p = -\frac{8}{\rho}\left[\frac{2+\rho}{6}\right]^{3/2}. \tag{5.18a,b}$$

In figure 6(*a*) we show the relation (5.18*b*) which defines two critical values of ρ for every $p < -2$. Within the region of the (ρ, p)-plane delimited by these two values (shown shaded in figure 6*a*), the polynomial in (5.16) has a root with $c_i > 0$. Elsewhere (in the unshaded region of figure 6*a*), the roots of (5.16) have negative imaginary parts so that there are no discrete modes. Thus in the unshaded region the profile is stable with a continuous spectrum.

The introduction of ρ enables us to condense the number of independent parameters from three (k, f, p), to two (ρ, p). But it is then difficult to visualize the region of instability in terms of the quantities with the most physical meaning. Thus, at the risk of redundancy, in figure 6(*b*) we show the corresponding stability boundary in the (k, p)-plane for three values of f. The profile is unstable in the region below the curves in figure 6(*b*).

According to equation (5.18) and figure 6(*a*), instability extends up to $p = -2$. At that point of marginality, $\rho(-2) = 4$ and so we have a critical wavenumber, k_c,

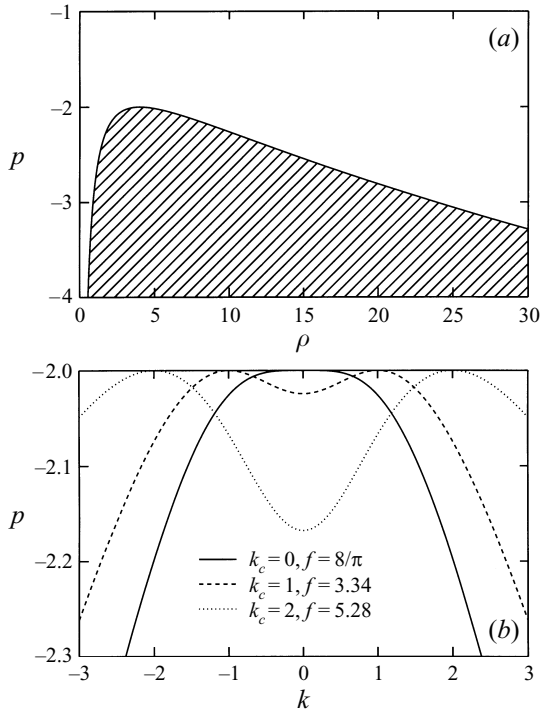

FIGURE 6. (*a*) The region of the (p, ρ) plane in which the polynomial (5.16) has a solution with $c_i > 0$ is shown shaded. (*b*) Stability boundaries in the (k, p)-plane for several values of $f \geqslant 8/\pi$.

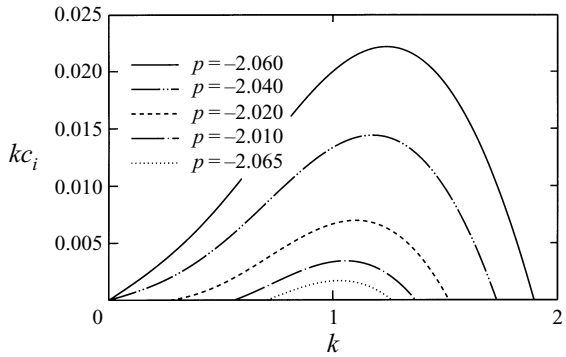

FIGURE 7. Growth rate, kc_i, as a function of k for profiles with indicated values of p obtained by solving the cubic equation (5.16). In all cases $f = 8\coth(1)/\pi = 3.34$.

defined as a function of f:

$$f = \frac{8}{\pi} k_c \coth k_c. \tag{5.19}$$

It follows from (5.19) that when $f < 8/\pi$ there is no instability. When $f > 8/\pi$, there may be a band of unstable wavenumbers centred on a finite value, and in figure 7 we show growth rate, $\omega_i = kc_i$ as a function of k with $f = 8\coth(1)/\pi$ and various values of p.

The instability described in this subsection is analogous to the 'bump-on-tail'

instability of plasma physics. The terminology is evident from figure 5 which shows how the splitting of the double inflection point results in a bump on the tail of the vorticity profile.

6. Stability theory for general vorticity defects

In the previous section we calculated the dispersion relation for various defect vorticity profiles, $F(\eta)$, and found several qualitatively different types of modal instability. To avoid the calculation of a dispersion relation every time a new profile is encountered, it is worth developing general results for classifying profiles according to their stability properties. We show in this section that a complete qualitative understanding of the modal stability problem can be obtained by using a variant of the Nyquist method (Penrose 1960).

We begin by introducing the dispersion function,

$$\mathscr{D}(c,k) \equiv 2k\coth k - \int_{-\infty}^{\infty} \frac{F'(\eta)}{\eta - c}\mathrm{d}\eta. \tag{6.1}$$

For each k, the equation above defines a function, $\mathscr{D} = \mathscr{D}_r + \mathrm{i}\mathscr{D}_i$, of $c = c_r + \mathrm{i}c_i$. The dispersion relation in (5.4) then corresponds to a zero of $\mathscr{D}$ in the c–plane. In view of our interest in unstable modes, which correspond to zeros of $\mathscr{D}$ in the upper half of the c–plane, we take $c_i > 0$ in what follows.

Except on the real axis, where the integral in the definition (6.1) is irregular, $\mathscr{D}$ is a bounded function of c. In fact, $\mathscr{D}$ is analytic in c except along the c_r-axis where it has a branch cut. However, using the Plemelj relation, we observe that as $c_i \downarrow 0$, $\mathscr{D}$ has the limiting value

$$\mathscr{D}(c_r,k) = 2k\coth k - \mathscr{P}\int_{-\infty}^{\infty} \frac{F'(\eta)}{\eta - c_r}\mathrm{d}\eta - \mathrm{i}\pi F'(c_r), \tag{6.2}$$

where $\mathscr{P}$ denotes a Cauchy principal value.

Because $\mathscr{D}(c,k)$ has no poles in the c-plane, the number of zeros of $\mathscr{D}(c,k)$ in the upper half-plane is given by

$$\frac{1}{2\pi\mathrm{i}}\int_{\gamma}\frac{1}{\mathscr{D}}\frac{\partial\mathscr{D}}{\partial c}\mathrm{d}c = \frac{1}{2\pi\mathrm{i}}\int_{\gamma'}\frac{\mathrm{d}\mathscr{D}}{\mathscr{D}}. \tag{6.3}$$

The contour of integration, γ, is a semicircle of infinite radius lying in the upper half of the c-plane, with a diameter limiting to the real axis from above; γ' is the image of γ in the $\mathscr{D}$-plane. According to (6.3) the number of unstable modes equals the number of times γ' encircles the origin in the $\mathscr{D}$-plane. Thus, to ascertain stability we need to know the shape of γ'. There are some straightforward considerations (illustrated in figures 8–11) that simplify this task.

The image of the whole semicircular arc of γ is the single point

$$\mathscr{D}_r + \mathrm{i}\mathscr{D}_i = 2k\coth k, \tag{6.4}$$

in the $\mathscr{D}$-plane. We refer to this point as the *asymptote*, and we use the notation $G(k) \equiv 2k\coth k$. The other part of γ is the real axis of the c-plane. The image of this segment gives γ' which departs from the asymptote, wanders in the $\mathscr{D}$-plane, and eventually returns to the asymptote. Equation (6.2) implies the following rules that constrain the topology of γ' using only qualitative properties of the defect vorticity profile:

(i) The direction in which γ' leaves and returns to the asymptote is determined by the sign of $F'(c_r)$ as $c_r \to \pm\infty$; e.g. if $F'(-\infty) > 0$, then γ' leaves the asymptote into the lower half-$\mathscr{D}$-plane, and so forth.

(ii) In addition to the asymptote, γ' can only cross the $\mathscr{D}_r$-axis at points for which $F'(c_r) = 0$; that is, at $c_r = \eta_n$ where η_n is one of the $n = 1, 2, \cdots N$ inflection points of the profile.

(iii) The crossings of γ' on the $\mathscr{D}_r$-axis are located at

$$d_n = 2k \coth k - \int_{-\infty}^{\infty} \frac{F(\eta) - F(\eta_n)}{(\eta - \eta_n)^2} \mathrm{d}\eta. \tag{6.5}$$

(iv) The direction in which γ' crosses the $\mathscr{D}_r$-axis at d_n is determined by the sign of $F''(\eta_n)$. If $F''(\eta_n) = 0$, then γ' touches the $\mathscr{D}_r$-axis but does not cross it. (This rule must be modified in obvious ways if higher derivatives such as $F'''(\eta_n)$ are zero.)

(v) If η_n is the global minimum (maximum) of $F(\eta)$ then d_n is to the left (right) of the asymptote. This follows from (6.5).

Next, we can vary k, and this affects only the location of the asymptote, $G(k)$. The function $2k \coth k$ increases monotonically from 2 as we raise k; hence increasing k drags γ' from its leftmost position at $k = 0$ to the right. This simple image enables us to decide if γ' will ever encircle the origin, O. For example, if at $k = 0$, the locus γ' does not cross the $\mathscr{D}_r$-axis to the left of O, then γ' can never encircle O at any value of k and the profile is stable. But if at $k = 0$, γ' does cross the $\mathscr{D}_r$-axis to the left of O then there must be some value of k for which O is encircled. This follows since the origin is either encircled at $k = 0$, or there is an even number of crossings to the left of O. In the former case the profile is unstable at $k = 0$. In the latter circumstance, increasing k drags γ' to the right until two crossings straddle O and consequently γ' encircles O. Hence there is instability centred on a finite value of k.

The action of varying k and dragging γ' to the right therefore allows us to determine the bands of unstable wavenumbers. These must be delimited by the values of k for which γ' passes through the origin. In other words, if $d_n = 0$, we must have a stability boundary.

For profiles with a single inflection point, the rules imply that γ' is a single loop. The locus γ' crosses the $\mathscr{D}_r$-axis at the asymptote, and at d_1 which is the image of the inflection point $c_r = \eta_1$. If η_1 is a maximum (figure 8*a*), then γ' circulates to the right of the asymptote (figure 8*b*) and the origin is never encircled. Therefore, single-humped, positive-vorticity defects are always stable (a restatement of the Fjørtoft extension of Rayleigh's Theorem). On the other hand, when η_1 is a minimum (figure 8*c*), γ' circulates to the left of the asymptote (figure 8*d*). Then, if $d_1 < 0$, the origin is encircled and the profile is unstable. In this unstable case, as we vary k, we drag the loop to the right. At some value of k, the loop passes through the origin, and so for higher k, γ' cannot encircle the origin any more. In other words, as we increase k, we pass through a high-wavenumber cut-off. If we now reduce the size of the loop by varying the profile (by reducing the size of the minimum), we move this cut-off to smaller and smaller values of k. Eventually, instability cuts off entirely (cf. figure 4), and this necessarily occurs at $k = 0$. Thus the singly peaked profiles, if unstable, are marginal at $k = 0$.

For profiles with two inflection points, γ' crosses the $\mathscr{D}_r$-axis at two points away from the asymptote. In the example shown in figure 9, the crossing at d_1 is associated with the global vorticity minimum, and so it is located to the left of the asymptote. The crossing at d_2, being the global maximum, is to the right of the asymptote.

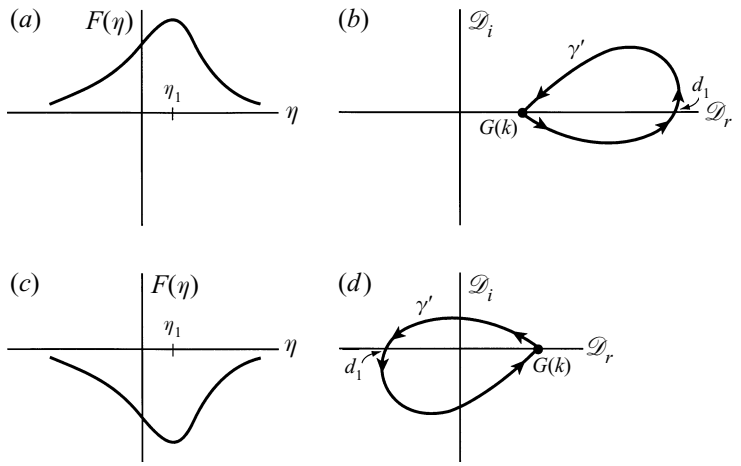

FIGURE 8. Nyquist plots for (*a*) positive, and (*c*) negative, vorticity defect profiles with a single inflection point. Because there is only one inflection point, γ' crosses the $\mathscr{D}_r$-axis twice: at the asymptote $G(k)$ denoted by a heavy dot, and at d_1, the image of η_1 in the $\mathscr{D}$-plane. In (*a*) η_1 is a global maximum and therefore γ' in (*b*) loops to the right of the asymptote. On the other hand, in (*c*) η_1 is a minimum and γ' in (*d*), loops to the left of the asymptote.

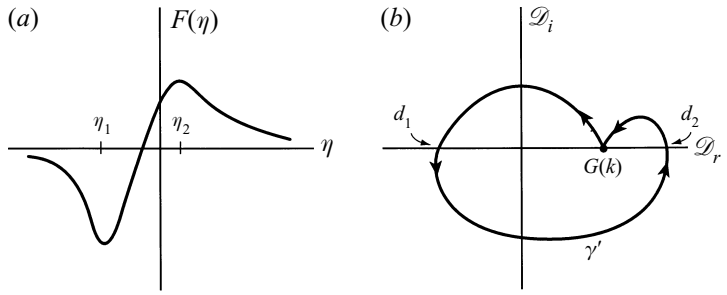

FIGURE 9. Nyquist plot for a vorticity defect profile with two inflection points. Because η_2 is a global maximum, the crossing d_2 is to the right of the asymptote. On the other hand, because η_1 is a minimum, the crossing d_1 is to left of the asymptote.

Instability occurs provided $d_1 < 0$. However, γ' can only encircle the origin at most once, so the profile in figure 9(*a*) can support only one unstable mode, and this is again marginal only at $k = 0$.

For profiles with three inflection points, there are yet more crossings of the $\mathscr{D}_r$-axis. Now the topology of γ' is less constrained and there are various ways in which γ' might encircle the origin. For example, the profile shown in figure 10(*a*) leads to a locus that does not encircle the origin for $k = 0$ (figure 10*b*). However, for large enough k, γ' is dragged to the right and encircles the origin. Figure 10(*c*) shows the profile for which the two inflection points at η_2 and η_3 coalesce and $F''(\eta_2) = 0$. In this critical case, γ' does not cross the $\mathscr{D}_r$-axis at $d_2 = d_3$, but touches it tangentially (figure 10*d*). There is then a critical wavenumber, k_c, at which the non-transversal intersection of γ' with the $\mathscr{D}_r$–axis is at the origin. In this case, any perturbation of the vorticity profile which moves the two coincident inflection points apart will open up an unstable band of wavenumbers centred on k_c (cf. figure 7).

Another interesting example with three inflection points is shown in figure 11. In this case, γ' encircles the origin twice over a range in k, and therefore there are two

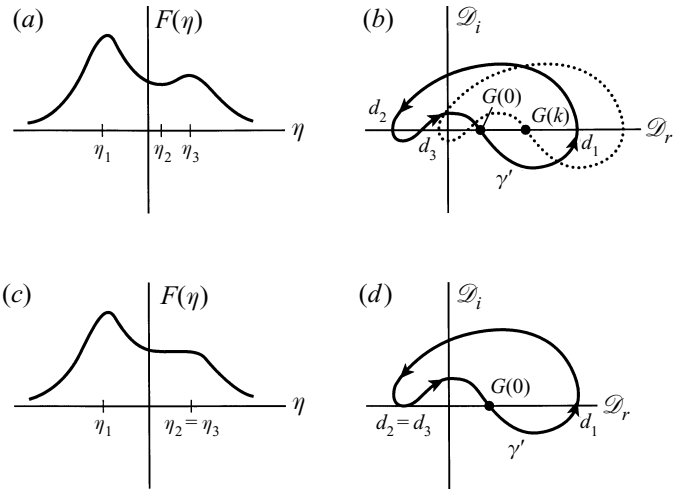

FIGURE 10. Nyquist plots for profiles with two maxima and one minimum. The profile shown in (*a*) is not unstable at $k = 0$ (see the solid curve in *b*), but there are two crossings, d_2 and d_3, to the left of the origin. Increasing k therefore drags γ' to the right so as to encircle the origin, as shown by the dotted curve in (*b*). (*c*) A case in which η_2 and η_3 have merged into a double inflection point with $F'' = 0$. In this case, as shown in (*d*), γ' does not cross the $\mathscr{D}_r$-axis and there is a point of marginal stability.

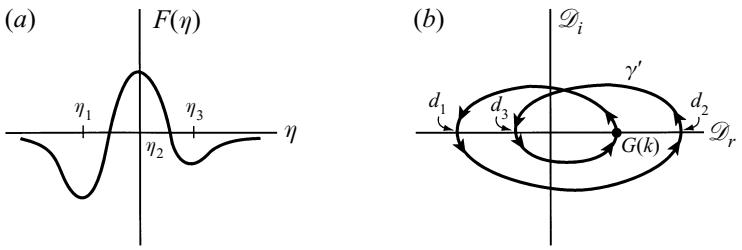

FIGURE 11. Nyquist plot for a profile with two minima and one maximum (*a*). In this case, γ' encircles the origin twice (*b*).

unstable modes. A concrete example of this double instability is provided by the vorticity profile $F(\eta) = f(1-\eta^2)/(1+\eta^2)^2$ which is the member $(p, q) = (0, -1)$ of the family in (5.14). Consideration of the dispersion relation (5.15) shows that the profile has two modes of instability if $f > 8/\pi$. Because of the symmetry of the vorticity profile the two modes are simultaneously marginal at $f = 8/\pi$.

With Nyquist plots we can categorize all of the bifurcations that can take place as we scan through a family of profiles. In particular we can understand the stability boundaries for the family. This naturally leads us to a necessary and sufficient criterion for modal instability. Namely, the profile is unstable if and only if there is at least one inflection point, η_n, with $F''(\eta_n) \neq 0$, for which

$$\int_{-\infty}^{\infty} \frac{F(\eta) - F(\eta_n)}{(\eta - \eta_n)^2} \, \mathrm{d}\eta > 2. \tag{6.6}$$

The inequality above ensures that when $k = 0$ there is at least one crossing point, d_n, to the left of the origin. Hence, for some k, γ' must encircle the origin at least once. The criterion (6.6) is the analogue of the Penrose criterion in plasma physics (Penrose

1960) and, for profiles with a single inflection point, (6.6) is equivalent to Rosenbluth & Simon's (1964) necessary and sufficient condition for instablity.

It is also clear from the Nyquist plots that there can only be as many unstable modes as inflection points, which repeats Howard's (1964) theorem for monotonic velocity profiles. In fact, we can make a much stronger statement than this. In order to encircle the origin, we need *two* crossings of the $\mathscr{D}_r$-axis. Hence the number of times γ' encircles the origin in total cannot exceed half of the number of times γ' intersects the $\mathscr{D}_r$-axis. The number of intersections is given by the number of inflection points plus the asymptote; that is $N+1$. Thus, the total number of unstable modes cannot exceed $(N+1)/2$.

7. The initial-value problem

In §5 we obtained the regular normal modes (the *discrete spectrum*) of the linearized vorticity defect equation for a number of basic states. This approach is limited because these normal modes do not form a complete set. Indeed, some of the stable profiles in §5 have no discrete modes. Thus, the solution of the initial-value problem demands the *continuous spectrum* in order to represent an arbitrary disturbance (Case 1960). In this section we follow this route and study the evolution of a small disturbance,

$$\zeta(x,\eta,0)=\zeta_0(x,\eta), \tag{7.1}$$

by solving the linearized equation (5.2) as an initial-value problem with Laplace transforms. Unlike earlier applications of this technique to the Rayleigh equation (Case 1960), our solutions are explicit, and they concretely display the competition among the transient amplification of the continuum, its eventual decay, and the sustained growth of unstable normal modes.

7.1. *Growth and decay of disturbances on a Couette flow: $F(\eta)=0$*

We begin our study of the initial-value problem with the special case $F(\eta)=0$. For this case, the solution of the vorticity defect equation (5.2*a*), with initial condition (7.1), is (Kelvin 1887; Orr 1907)

$$\zeta(x,\eta,t)=\zeta_0(x-\eta t,\eta). \tag{7.2}$$

By substituting this solution into (5.2*b*), we find

$$\tilde{b}(k,t)=-\tfrac{1}{2}k^{-1}\tanh k\int_{-\infty}^{\infty}\mathrm{e}^{-\mathrm{i}kt\eta}\,\tilde{\zeta}_0(k,\eta)\,\mathrm{d}\eta. \tag{7.3}$$

The integral on the right-hand side of (7.3) is the Fourier transform in η of $\tilde{\zeta}_0(k,\eta)$ where kt is the transform variable. Therefore, the behaviour in time of the streamfunction, $\tilde{b}(k,t)$, is determined by the Fourier transform in η of the initial perturbation. For example, if

$$\zeta_0(x,\eta)=\frac{\mathrm{e}^{\mathrm{i}k_0x}}{1+\eta^2}\,, \tag{7.4}$$

then

$$b(x,t)=-\tfrac{1}{2}\pi k_0^{-1}\tanh k_0\;\mathrm{e}^{-|k_0t|}\mathrm{e}^{\mathrm{i}k_0x}. \tag{7.5}$$

If one sets the time origin at $t=t_0<0$, then (7.5) exhibits a transient exponential growth up to $t=0$, abruptly followed by an exponential decay of the perturbation when $t>0$.

Because the dependence on time of $b(x,t)$ depends on the Fourier transform of the initial vorticity perturbation one can manufacture qualitatively different examples of growth followed by decay. For example, if $\zeta_0 = \exp(-\eta^2 + \mathrm{i}k_0 x)$ then the analogue of (7.5) is $b \sim \exp(-k^2t^2/4)$, so that there is superexponential growth until $t = 0$, followed by superexponential decay. These examples show that there is no universal expression for the time dependence of the streamfunction $b(x,t)$. The one general result is that, provided the initial condition in (7.1) is infinitely differentiable in η, repeated integrations by parts in (7.3) shows that $b(x,t)$ vanishes faster than any power of t as $t \to \pm\infty$.

The transient growth described above is the classical result of Orr and Kelvin. Note however, that because of the defect localization the quasi-exponential transient in (7.5) is stronger than the algebraic behaviour associated with the shearing of a uniform plane wave.

The conclusion that b decays faster than any power of t contrasts sharply with the well-known result that the streamfunction of a perturbation to a stable shear flow decays as t^{-2} (e.g. Brown & Stewartson 1980). This contradiction is resolved at next order in the expansion of the streamfunction within the defect; that is, by the term, $\varphi_1(x,\eta,t)$, in (3.11a). If we substitute solution (7.2) into (3.13), then we obtain

$$\varphi_{1\eta\eta} = \zeta_0(x - \eta t, \eta)\ . \tag{7.6}$$

We first take the Fourier transform in x of (7.6) and then follow Brown & Stewartson by substituting $\tilde{\varphi}_1(k,\eta,t) = \theta(k,\eta,t)\mathrm{e}^{-\mathrm{i}k\eta t}$, so that

$$\theta_{\eta\eta} - 2\mathrm{i}kt\theta_\eta - k^2t^2\theta = \tilde{\zeta_0}. \tag{7.7}$$

In the limit $t \to \infty$, the leading-order solution of (7.7) is $\theta \approx -\tilde{\zeta}_0/(kt)^2$, which is the universal law for algebraic decay of the streamfunction.

Thus, the solution of the $F(\eta) = 0$ problem using the vorticity defect approximation leads us to conclude that the streamfunction of a localized disturbance in Couette flow is, to leading order, composed of two parts. The dominant part, $b(x,t)$, has a non-universal time dependence and, provided that the initial condition is smooth, $b(x,t)$ decays faster than any power of t. The second, smaller (by one power in ϵ) correction, $\varphi_1(x,\eta,t)$, has a milder time dependence and contains the universal asymptotic decay, t^{-2}. Because of the different rates of decay, the expansion $\psi = b(x,t) + \epsilon\varphi_1(x,\eta,t) + O(\epsilon^2)$ becomes disordered as $t \to \infty$.

7.2. *Disturbances on a state with non-zero vorticity: $F(\eta) \neq 0$*

To study the case with non-zero $F(\eta)$ we use the Fourier–Laplace transform

$$\hat{\zeta}(k,\eta,p) \equiv \int_{-\infty}^{\infty} \mathrm{d}x \int_0^{\infty} \mathrm{d}t\, \zeta(x,\eta,t)\, \mathrm{e}^{-\mathrm{i}kx - pt}, \tag{7.8}$$

where $p = p_r + \mathrm{i}p_i$. The convergence of the t-integral in (7.8) requires that $p_r > p_0$ where p_0 is a real number. The 'abscissa of convergence' is the smallest value of p_0 for which the t-integral converges. The t-integral defines an analytic function of p in the half-plane of convergence, $p_r > \min(p_0)$. The Laplace transform is the analytic continuation into the whole of the p-plane of the function defined by the t-integral. Outside the half-plane of convergence, the Laplace transform may have singularities (see Pipkin 1991). These technicalities will be important in what follows.

The solution of the transformed version of (5.2) is

$$\hat{b}(k,p) = \frac{\mathscr{N}}{\mathscr{D}}, \quad \hat{\zeta}(k,\eta,p) = \frac{\tilde{\zeta}_0 - \mathrm{i}kF'\hat{b}}{p + \mathrm{i}k\eta}, \tag{7.9a,b}$$

where

$$\mathscr{N}(k,p) \equiv \frac{\mathrm{i}}{k}\int_{-\infty}^{\infty} \frac{\tilde{\zeta}_0}{\eta - \mathrm{i}p/k}\mathrm{d}\eta, \quad \mathscr{D}(k,p) \equiv 2k\coth k - \int_{-\infty}^{\infty} \frac{F'}{\eta - \mathrm{i}p/k}\mathrm{d}\eta. \tag{7.10a,b}$$

The function $\mathscr{D}$ in (7.10*b*) is equivalent to the dispersion function, $\mathscr{D}(k,c)$, introduced in §6, if $c = \mathrm{i}p/k$. Equations (7.9) and (7.10) determine $\hat{\zeta}(k,\eta,p)$ and $\hat{b}(k,p)$ in terms of the vorticity distribution $F(\eta)$ of the basic state, and the initial vorticity perturbation, $\tilde{\zeta}_0(k,\eta)$. Note that $\mathscr{D}$ depends only on the basic state, $F(\eta)$, whereas $\mathscr{N}$ depends only on the initial perturbation, $\zeta_0(x,\eta)$. The inversion formula for the Laplace transform of the streamfunction is

$$\tilde{b}(k,t) = \frac{1}{2\pi\mathrm{i}}\int_{p_0-\mathrm{i}\infty}^{p_0+\mathrm{i}\infty} \frac{\mathscr{N}}{\mathscr{D}}\,\mathrm{e}^{pt}\,\mathrm{d}p, \tag{7.11}$$

where the integration is along the Bromwich contour which is a straight line parallel to the imaginary p-axis and located to the right of the abscissa of convergence. An analogous expression determines $\tilde{\zeta}(k,\eta,t)$ from $\hat{\zeta}(k,\eta,p)$.

After the analytic continuation of the integrand of (7.11) into the right half of the p-plane has been performed, (7.10) and (7.11) are equivalent to Landau's celebrated solution of the initial value problem for the Vlasov equation (Landau 1946). Landau gave a prescription for accomplishing this analytic continuation for general functions $\tilde{\zeta}_0$ and F in (7.10) (for example, see Nicholson 1983). We will not need this Landau prescription in its full glory; rather we perform the continuation for specific illustrative examples. The essential point is that Landau's analytic continuation uncovers the singularities of $\hat{b}(k,p)$ which lie to the left of the abscissa of convergence. With the Cauchy residue theorem, knowledge of these singularities simplifies the evaluation of the inversion integral in (7.11) (Pipkin 1991). The uncovered singularities of $\hat{b}(k,p)$ arise from either the denominator, $\mathscr{D}$, or the numerator, $\mathscr{N}$, of the integrand in (7.11).

The poles arising from the denominator in (7.11) are the zeros of $\mathscr{D}$, and these are of two types depending on the sign of p_r. The zeros of $\mathscr{D}$ with $p_r > 0$ correspond to the unstable normal modes discussed in §5: the residues of these poles provide exponentially growing contributions in $b(x,t)$. The zeros of $\mathscr{D}$ with $p_r < 0$, however, are not the stable normal modes to which the unstable eigenvalues are complex conjugates. This is because, as we have seen before, the function $\mathscr{D}$ contains a potentially singular integral. That integral defines a function with a branch cut along the p_i-axis. The analytic continuation of the integral into the left-half-plane passes through this branch cut, and so to remain on the Riemann surface we must evaluate $\mathscr{D}$ on a different Riemann sheet. Thus the zeros of $\mathscr{D}$ in the left-half-plane are not solutions to the dispersion relation, but are zeros of its analytic continuation (the distinction becomes more obvious for the explicit example described below). The resulting singularities in $\hat{b}$ are the so-called 'Landau poles', whose residues contribute exponentially decaying contributions to $b(x,t)$. This is the fluid analogue of *Landau damping*.

Singularities in $\hat{b}$ can also be due to singularities in $\mathscr{N}$ (cf. Weitzner 1963). We restrict attention to the case in which the singularities of $\mathscr{N}$ are poles, and we refer to these as $\mathscr{N}$-poles. The $\mathscr{N}$-poles have not been widely discussed in either plasma

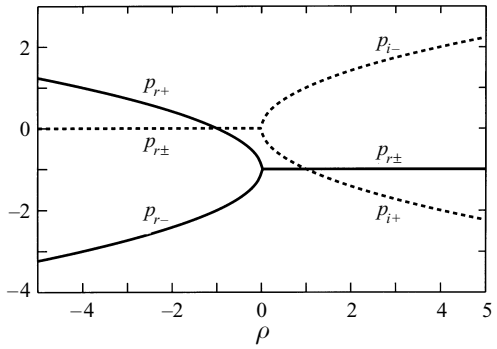

FIGURE 12. Zeros ($p_\pm = p_{r\pm} + \mathrm{i}p_{i\pm}$) of the function $\mathscr{D}$ for the Lorentzian basic state, as function of ρ, for $k = 1$. For $\rho < -1$, the basic state is unstable and the branch p_{r+} gives the growth rate of the unstable normal mode found in §5. The other branches, including p_{r+} for $\rho > -1$, are the Landau poles.

physics or fluid dynamics; indeed there is no accepted term for these objects. Perhaps this is because Landau restricted attention to initial conditions for which ζ_0 is an entire function of the complex variable η. This means that $\mathscr{N}$ has no singularities. However, these analyticity requirements are too restrictive; indeed, the initial condition we will use in (7.15) has poles at $\eta = \pm\mathrm{i}$.

In what follows we will present several examples which illustrate the interplay among unstable normal modes, Landau poles, and $\mathscr{N}$-poles.

7.3. *The initial-value problem for the Lorentzian*

To illustrate the previous generalities, we now present an explicit solution of the initial-value problem for the Lorentzian vorticity distribution, $F(\eta) = f/(1+\eta^2)$. For this basic state, evaluation of the integral $\mathscr{D}$ in (7.10*b*), for p to the right of the abscissa of convergence, gives

$$\mathscr{D}(k,p) = \frac{2k\coth k}{(p+k)^2}\,(p-p_+)(p-p_-), \tag{7.12}$$

where

$$p_\pm \equiv -(1 \pm \mathrm{i}\rho^{1/2})\,|k|, \quad \rho \equiv \pi f \tanh k/2k\ . \tag{7.13}$$

The analytic continuation into the region to the left of the abscissa of convergence is now accomplished by declaring that (7.12) defines a function of p everywhere in the p-plane.†

On substituting (7.12) into (7.11) we obtain

$$\tilde{b}(k,t) = \frac{\tanh k}{4\pi\mathrm{i}k}\int_{p_0-\mathrm{i}\infty}^{p_0+\mathrm{i}\infty} \frac{(p+k)^2\mathscr{N}}{(p-p_+)(p-p_-)}\,\mathrm{e}^{pt}\,\mathrm{d}p. \tag{7.14}$$

If $\mathscr{N}$ has no singularities then the only poles of the integrand are $p_\pm$ and the time evolution of the initial perturbation is of the form $\tilde{b} \propto R_-\mathrm{e}^{p_- t} + R_+\mathrm{e}^{p_+ t}$, for some $R_\pm$. Figure 12 shows $p_\pm = p_{r\pm} + \mathrm{i}p_{i\pm}$ as function of ρ. According to the results on §5, when $\rho < -1$ the basic profile is unstable. Indeed the branch p_{r+} with $\rho < -1$ in figure 12

† The integral in (7.10*b*) produces the expression in (7.12) only if $p_r > 0$. The analytic continuation of (7.12) (which amounts to ignoring the restriction that $p_r > 0$) passes through this branch cut. Hence the zeros of (7.12) with $p_r < 0$ lie through the cut on a different Riemann sheet and are uncovered by analytic continuation.

corresponds to the unstable normal mode of §5. The other branches in figure 12, with $p_r < 0$, are Landau poles.

7.4. *Instability and Landau damping*

We now consider the evaluation of (7.14) for a family of initial perturbations given by

$$\zeta_0(x,\eta) = -\frac{2\eta}{(1+\eta^2)^2}\mathrm{e}^{\mathrm{i}k_0 x + \mathrm{i}l_0\eta}. \tag{7.15}$$

If $l_0 = 0$ then ζ_0 is an antisymmetric function of η and thus (7.15) corresponds to a sinuous deformation of the Lorentzian vorticity distribution. The parameter l_0 can be used to produce additional sinusoidal structure in the η-direction. When k_0 and l_0 have the same sign this sinusoidal structure tilts backwards against the Couette shear flow. The mechanism of Orr and Kelvin suggests that this backwards tilt should produce substantial transient growth. Accordingly, we will assume that k_0 and l_0 are both positive.

By substituting (7.15) into (7.10*a*), evaluating the integral assuming $p_r > 0$, and putting the result into (7.14), we arrive at the relation,

$$\tilde{b}(k,t) = -\tfrac{1}{2}\pi\delta(k-k_0)\tanh k_0 \int_{p_0-\mathrm{i}\infty}^{p_0+\mathrm{i}\infty} \frac{\Xi(k,l_0,p)\ \mathrm{e}^{pt}}{(p-p_+)(p-p_-)}\mathrm{d}p, \tag{7.16}$$

where

$$\Xi(k,l_0,p) \equiv \mathrm{e}^{-l_0}\left[\frac{(k+p)^2[k+l_0(k-p)]}{k(k-p)^2}\right] - \mathrm{e}^{-l_0 p/k}\left[\frac{4kp}{(k-p)^2}\right]. \tag{7.17}$$

Consider first the special case with $l_0 = 0$. In this case $\Xi = 1$, and the inversion of the transform in (7.16) provides

$$b(x,t) = \frac{\pi}{4}\frac{\tanh k_0}{k_0\rho_0^{1/2}}\left(\mathrm{e}^{p_+ t} - \mathrm{e}^{p_- t}\right)\mathrm{e}^{\mathrm{i}k_0 x} \tag{7.18}$$

and

$$\zeta(x,\eta,t) = -\frac{2\eta\rho_0 k_0 \coth k_0}{\pi\kappa_+\kappa_-(1+\eta^2)^2}\left[2(1+\kappa_+\kappa_-)\mathrm{e}^{-\mathrm{i}k_0\eta t} + \left(\kappa_-\mathrm{e}^{p_- t} - \kappa_+\mathrm{e}^{p_+ t}\right)\right]\mathrm{e}^{\mathrm{i}k_0 x}, \tag{7.19}$$

where

$$\kappa_\pm \equiv \frac{(\eta \pm \rho_0^{1/2}) + i}{\rho_0^{1/2}}, \tag{7.20}$$

and $\rho_0 \equiv \rho(k_0)$. Equations (7.18) and (7.19) are the complete solution of the linear evolution problem with $l_0 = 0$. Figure 13 displays the time evolution of the streamfunction in (7.18) evaluated at $x = \pi/2$ for $k_0 = 1$ and different values of ρ.

If $\rho > -1$ then,the vorticity profile is stable and there are no regular normal modes. In this case the solution contains only Landau poles, and the streamfunction decays exponentially through Landau damping. By contrast, in the vorticity (7.19), the term proportional to $\exp(\mathrm{i}k_0\eta t)$ remains as $t \to \infty$. This is a sheared disturbance similar to the Couette solution considered earlier. Thus, over a sufficiently long time, all that remains of the initial perturbation is an increasingly sheared vortical remnant, like that shown in figure 14. Note that, even though the solution (7.18) and (7.19) contains exponentials of the form $\exp(p_\pm t)$, these are *not* normal-mode solutions except when $p_+ > 0$ ($\rho < -1$). In fact, because of the terms involving $\exp(-\mathrm{i}k_0\eta t)$, (7.19) does

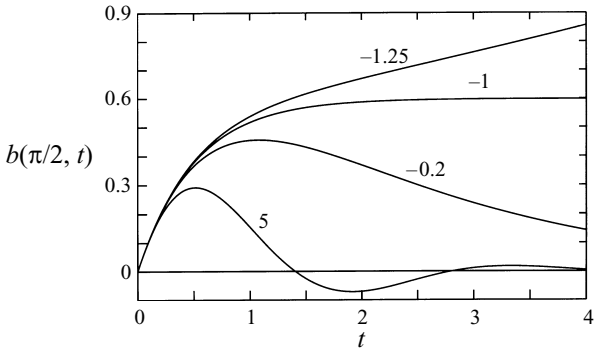

FIGURE 13. Time evolution of the streamfunction b at $x = \pi/2$ calculated from (7.18) with $k_0 = 1$. The number on each curve denotes the different values of ρ considered. The profile with $\rho = -1.25$ is unstable and in this case b grows exponentially after a transient. In the other cases the profile is stable and the streamfunction perturbation Landau damps. The corresponding evolution for the vorticity when $\rho = -0.2$ is shown in figure 14.

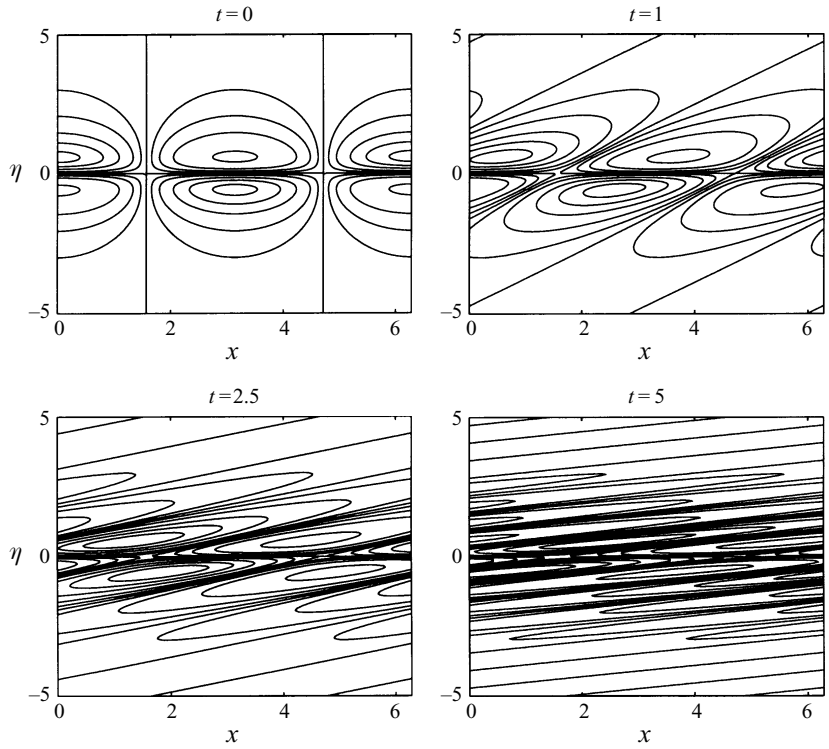

FIGURE 14. Contour plots showing the vorticity $\zeta(x, \eta, t)$ for $\rho = -0.2$, and $k_0 = 1$, calculated from (7.19).

not have separable structure, $\zeta(x, \eta, t) = \mathscr{Z}(\eta)\exp[\mathrm{i}k(x - ct)]$; thus the normal-mode ansatz in §5 does not capture these exponentially decaying structures. In plasma physics these objects are known as 'quasi-modes'; they are coherent excitations of the continuous spectrum.

When $\rho < -1$, the profile is unstable, and (7.18) and (7.19) can be rewritten as

$$b(x,t) = -\mathrm{i}\frac{\pi}{4}\frac{\tanh k_0}{k_0|\rho_0|^{1/2}}\left[\mathrm{e}^{\mathrm{i}k_0(x-ct)} - \mathrm{e}^{\mathrm{i}k_0x+p_-t}\right], \tag{7.21a}$$

$$\zeta(x,\eta,t) = \frac{1}{2}\frac{F_\eta}{\eta - c}\mathrm{e}^{\mathrm{i}k_0(x-ct)} + F_\eta\left[\frac{1+\kappa_+\kappa_-}{\kappa_+\kappa_-}\mathrm{e}^{-\mathrm{i}k_0\eta t} - \frac{\mathrm{e}^{p_-t}}{2\kappa_-}\right]\mathrm{e}^{\mathrm{i}k_0x}, \tag{7.21b}$$

where $c = \mathrm{i}p_+/|k_0|$ is the phase speed of the unstable normal mode found in (5.13). The terms involving $\exp[\mathrm{i}k_0(x-ct)]$ in (7.21) are simply multiples of the unstable eigenfunction in (5.3). In other words, as expected, the solution contains the unstable mode. The other exponential, $\exp(p_-t)$, is *not* the contribution of the decaying mode to which the unstable eigenfunction is paired by complex conjugation, i.e. $p_- \neq c^*$. In fact, once again, the decaying exponential $\exp(p_-t)$ is an example of a quasi-mode.

7.5. *Tilted wave perturbations and transient growth*

We now return to (7.16) and consider the general case with $l_0 \neq 0$ so that Ξ in (7.17) has a second-order $\mathscr{N}$-pole at $p = k_0 > 0$. At first glance, this $\mathscr{N}$-pole is puzzling because its residue is proportional to $t\exp(k_0t)$ and this seems to imply that the perturbation will always grow, even if the profile has no unstable normal modes. However, the evaluation of the integral in (7.16) must be done in two stages. When $t < l_0/k_0$ one should split Ξ in (7.17) into two parts. The contribution from the part proportional to $\exp(-l_0p/k_0)$ is zero because this integral can be calculated by closing the Bromwich contour in the right-half-plane where there are no singularities. The second part, proportional to $\exp(-l_0)$, must be evaluated by closing the Bromwich contour in the left-half-plane. The resulting contour encloses the three poles at $p = p_\pm$ and $p = k_0$, and there is a non-zero residue contribution from all three. On the other hand, when $t > l_0/k_0$, one does not split Ξ, and the integral (7.16) is calculated by closing in the left-half-plane. In this case all three poles are enclosed. But now the residue of the $\mathscr{N}$-pole at $p = k_0$ is zero because of cancellations amongst the various terms in Ξ. The final result of the calculation described above is

$$b(x,t) = -\pi\mathrm{i}\frac{\tanh k_0}{2k_0}\mathrm{e}^{-l_0}\left(R_{k_0}\mathrm{e}^{k_0t} + R_{p_+}\mathrm{e}^{p_+t} + R_{p_-}\mathrm{e}^{p_-t}\right)\mathrm{e}^{\mathrm{i}k_0x} \quad \text{if} \quad 0 < t < l_0/k_0, \tag{7.22a}$$

$$b(x,t) = \frac{\pi}{4}\frac{\tanh k_0}{k_0\rho_0^{1/2}}\left[\Xi(k_0,l_0,p_+)\mathrm{e}^{p_+t} - \Xi(k_0,l_0,p_-)\mathrm{e}^{p_-t}\right]\mathrm{e}^{\mathrm{i}k_0x} \quad \text{if} \quad l_0/k_0 < t \tag{7.22b}$$

where

$$R_{k_0} \equiv \frac{4}{4+\rho_0}\left[k_0(t - l_0/k_0) + \frac{\rho_0}{4+\rho_0}\right], \quad R_{p_\pm} \equiv \mp\frac{\mathrm{i}\rho_0^{1/2}}{2}\frac{\left[1 + l_0(2 \pm \mathrm{i}\rho_0^{1/2})\right]}{(2 \pm \mathrm{i}\rho_0^{1/2})^2}. \tag{7.23a,b}$$

Note that (7.23*a*) is not well defined for $\rho_0 = -4$. For this value of ρ_0, $p_+ = k_0$ so that k becomes a third-order pole, and the residue has to be evaluated using a different expression.

The upshot of all this is that the growing term $t\exp(k_0t)$ appears only when $t < l_0/k_0$; that is, only when the perturbation wavefront is tilting against the shear. Thus, even though the profile is stable, there is strong transient growth for $t < l_0/k_0$. Thereafter, the growth gives way to Landau damping. In figure 15 we have plotted the solution in (7.22) at $x = \pi/2$, for $k_0 = 1$, and various values of ρ_0 and $l_0 = 5$. This figure displays the transient amplification that subsides into exponential decay, followed by the emergence of the unstable mode in the case for which it exists.

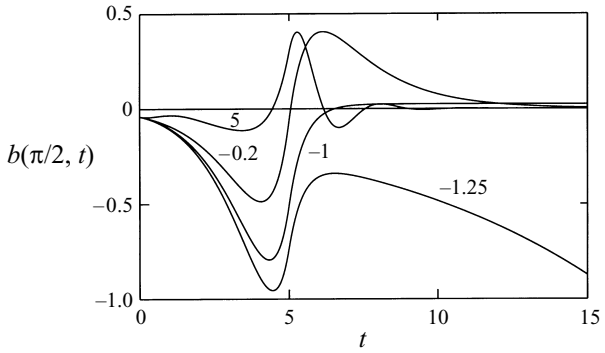

FIGURE 15. Time evolution of the streamfunction b at $x = \pi/2$ calculated from (7.22), for $\rho = 5$, -0.2, -1, and -1.25, with $k_0 = 1$ and $l_0 = 5$.

7.6. *Asymptotic $\mathcal{N}$-poles contributions*

In the examples presented above, the asymptotic ($t \to \infty$) decay of perturbations of a stable vorticity profile was determined solely by the Landau poles. However, this is not a general result. Consider the following family of initial perturbations to a Lorentzian profile:

$$\zeta_0(x, \eta) = \frac{F'}{\eta + \mathrm{i}\mu} \mathrm{e}^{\mathrm{i}k_0 x} , \tag{7.24}$$

where μ is a real number, and $F(\eta)$ is the Lorentzian basic state. On evaluating the integral for $\mathcal{N}$ in (7.10*a*) (with $p_r > 0$), and substituting the result into (7.14), we conclude

$$\tilde{b}(k, t) = -\frac{\mathrm{i}\rho}{(1 + |\mu|)^2} \delta(k - k_0) \int_{p_0 - \mathrm{i}\infty}^{p_0 + \mathrm{i}\infty} \frac{(p - |\mu|k)[p + (2 + |\mu|)k]}{(p + \mu k)(p - p_+)(p - p_-)} \mathrm{e}^{pt} \mathrm{d}p. \tag{7.25}$$

The pole at $p = -\mu k$ is an $\mathcal{N}$-pole.

If $\mu < 0$, the residue of the $\mathcal{N}$-pole at $p = -\mu k_0$ vanishes because of the term $(p - |\mu|k)$ in the numerator. In this case only the Landau poles $p_\pm$ contribute and, when the profile is stable, the perturbation decays by Landau damping. If $\rho < -1$ and $|\mu| = -p_-/k_0 - 2$ then the residue of the Landau pole at p_- also vanishes, and $\tilde{b} \propto \mathrm{e}^{p_+ t}$, where $p_+ = (-1 + |\rho|^{1/2})k_0$ is the unstable eigenvalue. This result is expected because, for these values of ρ and μ, the initial condition in (7.24) is precisely the unstable eigenfunction.

If $\mu > 0$, on the other hand, both the Landau poles $p_\pm$, and the $\mathcal{N}$-pole at $p = -\mu k$, have non-vanishing residues. Which of these contributions dominates over asymptotically long times depends on the values of ρ and μ. More precisely, when $-1 < \rho < 0$ the asymptotic behaviour is dominated by the $\mathcal{N}$–pole if $0 < \mu < 1 - |\rho|^{1/2}$. On the other hand, when $\rho > 0$, the asymptotic behavior is dominated by the $\mathcal{N}$-pole provided $0 < \mu < 1$. Thus, there are situations in which Landau damping is less important than the decay intrinsic to the form of the initial condition.

7.7. *To summarize*

This section has shown that the linear evolution of localized inviscid disturbances on a Couette flow can be described analytically in considerable detail. Some aspects of these solutions, such as the transient amplification and the eventual decay of the streamfunction, are well known. But, in addition to these commonplaces, the solutions

show that a full understanding of the linear initial value problem requires concepts such as Landau poles and $\mathscr{N}$-poles. These ideas come from plasma physics and have received little attention in fluid mechanics (however see Briggs, Daugherty & Levy 1970). This is probably because if one is dealing with the full linear problem then explicit solutions of the initial value problem can only be found in the case with $F(\eta) = 0$ (so that there are no Landau poles and no quasi-modes).

In any event, if the profile is stable and whatever the form of the initial condition (provided it is smooth), the leading-order streamfunction, $b(x,t)$, decays exponentially. This signifies that the term $b_x F_\eta$ of equation (5.2*a*) becomes exponentially small as $t \to \infty$. Thus, the linearized vorticity defect approximation, (5.2*a*), reduces to the Couette problem of §7.1 after a sufficiently long time. Consequently, the exponential decay of the streamfunction is only a feature of the leading order, and the next-order correction to the streamfunction, $\varphi_1(x,\eta,t)$, eventually decays as t^{-2} (Brown & Stewartson 1980).

The extent to which these defect results apply to non-localized perturbations of a general shear flow is an open question. Some recent experimental work using non-neutral plasmas as a laboratory analogue of inviscid two-dimensional fluid mechanics (Driscoll & Fine 1990) may be relevant. Experiments with this system (Pillai & Gould 1994) have shown that stable disturbances have an initial exponential decay which is then followed by a protracted algebraic decay.

Finally, we mention that it may be necessary to incorporate additional physics in the long-time limit. The vortical remnant that endures after the phase mixing of the continuum has an extremely filamentary structure. This may be susceptible to secondary instabilities (e.g. Killworth & McIntyre 1985; Haynes 1985, 1987, 1989). The production of small-scale structure also suggests that dissipative effects will become important. Both of these processes can be studied within the context of the vorticity defect approximation and in the next section we focus on the effects of viscosity.

8. The viscous problem

To this point we have dealt only with inviscid theory. In this penultimate section we turn to the consequences of dissipation. On restoring the dissipative terms, the linearized vorticity defect approximation is

$$\zeta_t + \eta\zeta_x + b_x F_\eta = -\alpha\zeta + \nu\zeta_{\eta\eta}, \tag{8.1a}$$

$$2\tilde{b}(k,t) = -k^{-1}\tanh k \int_{-\infty}^{\infty} \tilde{\zeta}(k,\eta,t)\,\mathrm{d}\eta. \tag{8.1b}$$

We now follow the development in §5 and attempt to find modal solutions by substituting $\zeta(x,\eta,t) = \exp(\mathrm{i}kx - \mathrm{i}\omega t)\mathscr{Z}(\eta)$ into (8.1). This leads us to the following eigenproblem:

$$\nu\mathscr{Z}_{\eta\eta} - \mathrm{i}k(\eta - c_\alpha)\mathscr{Z} = -\tfrac{1}{2}\mathrm{i}\tanh k\, F_\eta \int_{-\infty}^{\infty} \mathscr{Z}(\eta')\,\mathrm{d}\eta', \tag{8.2a}$$

$$\mathscr{Z}(\eta) \to 0 \quad \text{as} \quad |\eta| \to \pm\infty, \tag{8.2b}$$

where $c_\alpha = (\omega/k) + \mathrm{i}(\alpha/k)$ is the eigenvalue. Equation (8.2) is our approximation to the Orr–Sommerfeld problem for localized, viscous modes associated with the vorticity defect, $F(\eta)$.

It is clear that the Ekman friction plays a minor role in (8.2). In fact, by defining c_α

we have absorbed this process into a new eigenvalue c_α. That is to say, bottom drag uniformly shifts the spectrum in the direction of stability; we will now lighten our notation by taking $\alpha = 0$. Viscosity, however, is a singular perturbation and we spend this section exploring the ramifications of viscosity on the stability characteristics of defects.

8.1. *The Couette problem: $F(\eta) = 0$*

To solve (8.2), we need to first understand the eigenvalue spectrum of operator on the left-hand side. Hence, we initially consider the Couette problem, in which $F(\eta) = 0$ and

$$\nu \mathscr{Z}_{\eta\eta} - \mathrm{i}k(\eta - c)\mathscr{Z} = 0, \tag{8.3a}$$

$$\mathscr{Z}(\eta) \to 0 \quad \text{as} \quad |\eta| \to \pm\infty. \tag{8.3b}$$

The solutions of (8.3) are Airy functions of complex argument:

$$\mathscr{Z}(\eta) = a_1 \mathrm{Ai}\left[\kappa \mathrm{e}^{\mathrm{i}\pi/6}(\eta - c)\right] + a_2 \mathrm{Bi}\left[\kappa \mathrm{e}^{\mathrm{i}\pi/6}(\eta - c)\right], \tag{8.4}$$

where

$$\kappa = (k/\nu)^{1/3}, \tag{8.5}$$

and a_1 and a_2 are constants. Throughout this section we assume that $k > 0$ so that κ in (8.5) is a real positive constant. It follows from (8.2) that if $(k, c, \mathscr{Z})$ is an eigensolution then so is $(-k, c^*, \mathscr{Z}^*)$. This symmetry can be used to obtain the solutions with $k < 0$.

It is straightforward to observe from the asymptotic forms of the Airy functions for large argument (e.g. Abramowitz & Stegun 1972) that both independent solutions in (8.4) are unbounded in one of the limits, $\eta \to \pm\infty$. In other words, it is not possible to build a solution to (8.3*a*) that satisfies both of the boundary conditions in (8.3*b*) and we conclude that there are no regular eigenmodes.

The absence of normal-mode solutions to the Couette problem is connected to the fact that the linear viscous problem (8.1) is defined on an infinite domain. In a finite domain the Orr–Sommerfeld equation has a complete set of discrete normal modes. But in an unbounded domain we must anticipate the existence of a continuous spectrum (e.g. Murdock & Stewartson 1977).

In the present context the discrete spectrum is absent because the matched asymptotic expansion casts the inner problem on an infinite domain, $-\infty < \eta < \infty$, whereas the exact problem is defined on a finite domain, $-1 < y < 1$. In the case of bounded Couette flow the Airy functions in (8.4) can be used to build discrete eigenfunctions. However, at large Reynolds number these modes fall into two classes. There are relatively slowly decaying modes concentrated in boundary layers next to the walls (Davey 1973) and there are rapidly decaying modes with oscillatory structure in the centre of the channel (Schmid *et al.* 1992). The boundary modes are exponentially small in the main body of the flow, whereas the central modes are not localized within the defect region. Moreover, these central modes decay too rapidly to be seen over the long time scales assumed by our expansion in §2. Thus it is quite natural that the eigenvalue problem for Couette flow in (8.3) has no discrete modes; the complete set of discrete modes of the exact problem are ephemeral creatures of the outer flow and consequently they are filtered by the vorticity defect approximation. What remains, for general defect profiles, are modes that are directly associated with the vorticity defect.

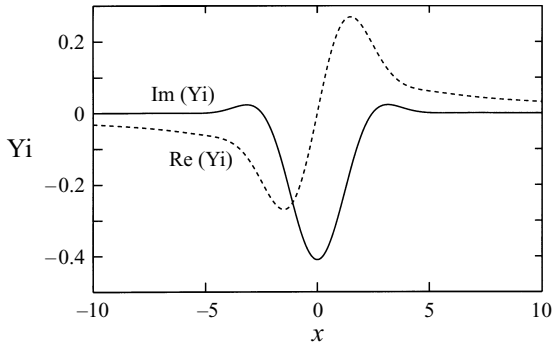

FIGURE 16. The Yi function on the real axis.

8.2. *The function* Yi(z)

Before turning to the solutions of (8.3) with non-zero $F(\eta)$ it is convenient to introduce a function

$$\mathrm{Yi}(z) \equiv -\frac{1}{\pi}\int_0^\infty \exp\left(-\tfrac{1}{3}v^3 - \mathrm{i}zv\right)\,\mathrm{d}v, \tag{8.6}$$

and collect some results which will form the basis of our investigation of the viscous problem. The function Yi is related to the special function Hi defined by Abramowitz & Stegun (1972, 10.4.44) by $\mathrm{Yi}(z) = -\mathrm{Hi}(-\mathrm{i}z)$. Also, Yi($z$) satisfies the inhomogeneous differential equation

$$\mathrm{Yi}'' - \mathrm{i}z\mathrm{Yi} = \frac{1}{\pi}. \tag{8.7}$$

We plot Yi(x), with x real, in figure 16.

We will also need to consider the asymptotic behaviour of Yi(z) when $|z|$ is large. This is given by

$$\mathrm{Yi}(z) \sim \frac{\mathrm{i}}{\pi z}\sum_{n=0}^{\infty}\frac{(3n)!}{3^n n!}(\mathrm{i}z)^{-3n} \quad \text{if} \quad \arg(z) < \tfrac{1}{6}\pi \text{ or } \tfrac{5}{6}\pi < \arg(z), \tag{8.8a}$$

and

$$\mathrm{Yi}(z) \sim \exp\left[\tfrac{2}{3}z^{3/2}\right] \quad \text{if} \quad \tfrac{1}{6}\pi < \arg(z) < \tfrac{5}{6}\pi. \tag{8.8b}$$

The asymptotic expansions in (8.8) show that if $z_r \to \pm\infty$, with z_i fixed, then $\mathrm{Yi}(z) \sim \mathrm{i}/\pi z$.

8.3. *The viscous dispersion relation*

The solution of the inhomogeneous equation

$$v\mathscr{L}^\dagger_{\eta\eta} - \mathrm{i}k(\eta - c)\mathscr{L}^\dagger = 1, \tag{8.9}$$

can be written in terms of Yi as

$$\mathscr{L}^\dagger(\eta; c, k, v) = \pi\kappa^{-2}v^{-1}\mathrm{Yi}\left[\kappa(\eta - c)\right]. \tag{8.10}$$

The function $\mathscr{L}^\dagger$ decays as $|\eta| \to \infty$; no matter what the value of c, as $|\eta|$ increases, the argument of the Yi function in (8.10) moves into the sector of the z-plane in which the asymptotic expansion in (8.8a) applies.

If we now multiply the eigenvalue problem (8.2) by $\mathscr{L}^\dagger$ and integrate, we obtain

$$\left[1 + \tfrac{1}{2}\mathrm{i}\tanh k \int_{-\infty}^{\infty} \mathscr{L}^\dagger F_\eta \,\mathrm{d}\eta\right] \int_{-\infty}^{\infty} \mathscr{L}\,\mathrm{d}\eta = 0. \tag{8.11}$$

One possible solution of (8.11) is $\int \mathscr{L}\,\mathrm{d}\eta = 0$. This is not, however, consistent with the eigenvalue problem; it implies that the right-hand side of (8.2) vanishes, and this would require a modal solution of the Couette problem, (8.4). Therefore,

$$1 = -\frac{\mathrm{i}\pi\kappa}{2k}\tanh k \int_{-\infty}^{\infty} \mathrm{Yi}\,[\kappa(\eta - c)]\, F_\eta(\eta)\,\mathrm{d}\eta. \tag{8.12}$$

The result in (8.12) is an explicit dispersion relation for the viscous eigenproblem in (8.2). It is remarkable that the dispersion relation can be obtained independently of the eigenfunctions.

8.4. *Viscous instabilities of the Lorentzian*

The dispersion relation (8.12) corresponds to a zero of the complex function

$$\mathscr{D}(c,k,\kappa) = 2k\coth k + \mathrm{i}\pi\kappa \int_{-\infty}^{\infty} \mathrm{Yi}\,[\kappa(\eta - c)]\, F_\eta(\eta)\,\mathrm{d}\eta. \tag{8.13}$$

The function $\mathscr{D}$ is analytic in the complex c-plane and therefore the Nyquist method can be used to establish necessary and sufficient conditions for instability. In particular, we may once more formulate the contour integral (6.3) used in the consideration of the inviscid problem to count the number of unstable modes. One can verify that $\mathscr{D}(R\mathrm{e}^{\mathrm{i}\theta}, k, \kappa) \to 2k\coth k + O(R^{-1})$ so that the image of the arc at infinite radius in the complex c-plane is once again the asymptote, $\mathscr{D} = 2k\coth k$. Thus, as before, if the image of the real c-axis, γ', encircles the origin of the complex $\mathscr{D}$-plane then there is an unstable mode.

To illustrate the viscous stability theory we again use the Lorentzian vorticity profile, $F(\eta) = f/(1+\eta^2)$. It turns out that with this choice the integral in (8.13) can be simplified by substituting the definition of Yi in (8.6), changing the order of integration, and then evaluating the integral over η. This procedure gives the dispersion function,

$$\mathscr{D}(c,k,\kappa) = 2k\coth k - \mathrm{i}\pi^2\kappa^2 f\,\mathrm{Yi}'[\kappa(-\mathrm{i} - c)] \tag{8.14a}$$

$$= 2k\coth k + \pi\kappa^2 f \int_0^{\infty} \mathrm{e}^{-v^3/3 - \kappa v + \mathrm{i}\kappa c v} v\,\mathrm{d}v. \tag{8.14b}$$

With numerical evaluation of Yi' in (8.14) we can readily construct the Nyquist plot (see figure 17) and determine if there is an unstable mode at a particular point in the (f, v, k) parameter space.

When $\rho \equiv \pi f \tanh k/2k < 0$, the locus has a single loop to the left of the asymptote, $\mathscr{D}(\pm\infty) = G(k)$ (figure 17*a*). Hence there is a bifurcation to instability at $c = 0$ when ρ is decreased through some threshold, exactly as in inviscid theory. This threshold is not, however, a simple function of wavenumber since k is contained in the dispersion function $\mathscr{D}(c,k,\kappa)$ in a more complicated way than in inviscid theory. In addition to determining the asymptote, k enters through the parameter $\kappa = (k/v)^{1/3}$, which we can view as an effective viscosity parameter. Complications arise because, although increasing k acts to shift the Nyquist plot to the right away from instability, the corresponding reduction in the effective dissipation acts to increase instability for the Lorentzian. Thus, in the viscous problem, there are two, k-dependent, competing

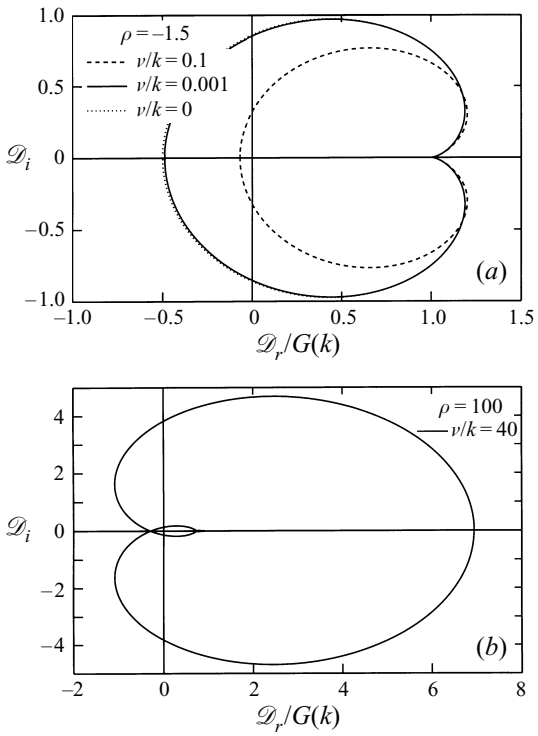

FIGURE 17. Nyquist plots calculated from (8.14). Notice that the horizontal axis is $\mathscr{D}/G(k)$ where $G(k) \equiv 2k \coth k$. This scaling puts the asymptote at $(1, 0)$ and ensures that the plot depends only on two parameters $(\rho, \nu/k)$. (*a*) If $\rho < 0$ then the Nyquist plot has a large rightward loop. (*b*) With $\rho > 0$ there are two small leftward loops emerging from the asymptote (the second, very small loop is not easily visible above).

influences on stability. One is essentially inviscid in nature, the other inherently dissipative. At large k, $G(k) \sim k$ whereas $\kappa \sim k^{1/3}$, so the inviscid influence dominates. As $k \to 0$, however, κ^{-1} diverges, so the viscous effect takes control for long waves. The result for the Lorentzian is a finite marginal wavenumber (see below).

When $\rho > 0$, we do not expect instability according to inviscid theory. Indeed, over much of the parameter space the main loop of the Nyquist plot passes to the right of the asymptote and there is no instability. However, there are also two smaller loops which lie to the left of the asymptote over a range of v. (The smallest loop is not conspicuous in figure 17*b*, but it is there.) For sufficiently large and positive values of ρ, these small leftward loops can encircle the origin. These enclosures show that there are two viscously catalyzed instabilities that are not anticipated by the inviscid theory.

The Nyquist method is a useful tool for determining if there is an unstable mode at some point in the (v, k, f) parameter space. We can also separate the real and imaginary parts of (8.14*b*) and take $c_i = 0$ to obtain rather simple expressions for the 'neutral surface' in this three-parameter space. After a change of variables this gives

$$0 = \int_0^\infty \exp\left[-\frac{v}{k}\frac{s^3}{3} - s\right] \sin(c_r s) s \mathrm{d}s, \tag{8.15a}$$

$$1 = -\rho(k, f) \int_0^\infty \exp\left[-\frac{v}{k}\frac{s^3}{3} - s\right] \cos(c_r s) s \mathrm{d}s. \tag{8.15b}$$

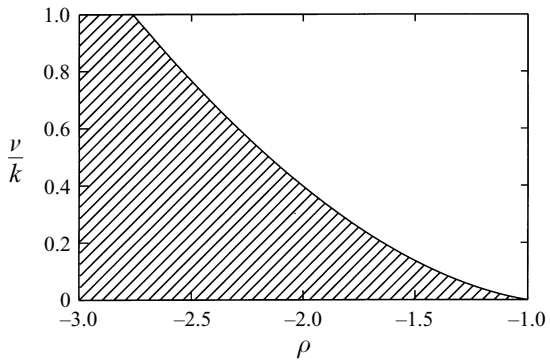

FIGURE 18. The shaded area below the neutral curve is the region in which there is a primary unstable mode corresponding to the Nyquist plot in figure 17(*a*). As $\nu \to 0$ the unstable region contacts to the point $(-1, 0)$ predicted by the inviscid theory.

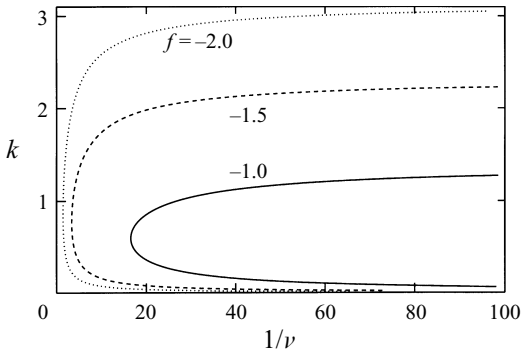

FIGURE 19. Neutral curves for the primary instability in the $(1/\nu, k)$ plane for $f = -1$, -1.5 and -2. As the defect Reynolds' number, $1/\nu$, becomes large, the upper limit of the band of unstable wavenumbers approaches the marginal inviscid wavenumber.

The eigenvalue, c_r, varies on the neutral surface, and from (8.15*a*) we see that c_r is a function only of the combination ν/k. Once (8.15*a*) has been solved, the result for c_r as a function of ν/k can then be inserted into (8.15*b*). This substitution shows that the neutral surface can be viewed as a curve in the $(\rho, \nu/k)$-plane. This reduces the number of independent parameters from three, (ν, f, k), to two, $(\rho, \nu/k)$.

There are two different types of neutral modes which emerge as solutions of (8.15). There are modes with $c_r = 0$, which are associated with the large rightward loop of the Nyquist plot in figure 17(*a*) and we refer to these modes as *primary* neutral modes. There are also solutions of (8.15) with $c_r \neq 0$. These *secondary* neutral modes are associated with the small leftward loops of the Nyquist plot in figure 17(*b*).

Figure 18 shows the neutral curve for the primary mode in the $(\rho, \nu/k)$-plane; the shaded region under the curve is unstable. For various values of f, we then find stability boundaries in the $(1/\nu, k)$-plane illustrated in figure 19. ($1/\nu$ is the 'defect Reynolds number'.) The boundaries in figure 19 exhibit two important features. First, with f fixed, the stability boundaries terminate at a critical value of ν, where there is a finite marginal wavenumber. Secondly, with fixed supercritical ν and fixed f, the profile is unstable over a band of wavenumbers; as $\nu \to 0$ this band of unstable wavenumbers expands until it spans the interval $(0, k_{inv})$, where k_{inv} is the inviscid neutral wavenumber.

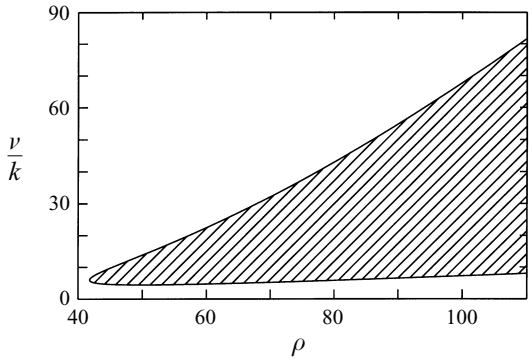

FIGURE 20. The shaded area enclosed by the neutral curve is the region in which there is a secondary unstable mode corresponding to the Nyquist plot in figure= 17(*b*).

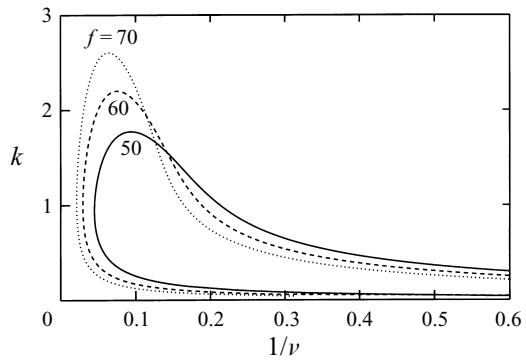

FIGURE 21. Neutral curves for viscous overstability in the $(1/v, k)$ plane for $f = 50$, 60 and 70. As the defect Reynolds' number, $1/v$, becomes large, the band of unstable wavenumbers narrows and approaches $k = 0$.

The viscous or secondary neutral modes are solutions of (8.15*a*) with $c_r \neq 0$. There are two such solution branches which correspond to the two leftward loops in the Nyquist plot in figure 17(*b*). Because $c_r \neq 0$ these modes are unstable travelling waves (the modes are 'overstable' according to Eddington's terminology). The threshold of instability for these viscous overstable modes then follows from substituting $c_r(v/k)$ into (8.15*b*) and computing the neutral curve in the $(\rho, v/k)$-plane. Figure 20 shows the neutral curve for the first of the two overstable branches; the shaded area is unstable. Figure 21 displays stability boundaries for various values of f. (The second overstable branch exists at even higher values of ρ and we do not display it.) An interesting feature of the secondary instabilities is that we may prolong them to arbitrarily small viscosities by taking k sufficiently small (see figure 21). In other words, instabilities appear whenever there is any viscosity at all, but not if there is no viscosity.

9. Concluding remarks

The evolution of small, localized vorticity bumps in a shear flow is concisely described by the vorticity defect approximation in (3.14). This equation has a simplified nonlinear term which is structurally identical to that of the Vlasov equation, and to the nonlinearity in the Stewartson (1978) and Warn & Warn (1978) forced critical

layer model. We believe that the vorticity defect approximation will ultimately prove to be a useful laboratory for investigating the nonlinear development of shear flow instabilities. As a necessary preliminary to those efforts, our main goal here has been to develop the linear theory in detail. It is largely in this sense that the present paper is a successor to, and a completion of, the work of Gill on small vortical distortions of Couette flow.

The linear theory of the vorticity defect approximation is analytically accessible to a surprising degree. For instance, we have presented explicit dispersion relations for the normal modes in both the inviscid and viscous cases, and we have used the Nyquist method to develop a qualitative understanding of the eigenvalue problem. The initial value problem has been solved using the Laplace transform and the resulting solutions display the interplay between phenomena intrinsic to the basic state (e.g. Landau poles and unstable normal modes) and other features which are accidents of the initial condition (e.g. $\mathscr{N}$-poles). Comparably explicit analytical results do not exist in the literature of shear flow stability.

Finally, there is another class of shear flow stability problems that we have avoided in constructing the vorticity defect approximation. These concern new issues that emerge when we allow the ambient shear to become non-monotonic. In that case there is the possibility of multiple defects that interact with one another. The defect analysis then gives coupled Vlasov-like equations for the defects, much as one handles differently charged species in Vlasov theory. There is also a special class of defects, namely those located near the points of vanishing shear, in which the whole inner problem changes. There results a completely different kind of temporal linear dynamics and nonlinear solutions (e.g. Brunet & Warn 1990; Brunet & Haynes 1995).

We thank Rupert Ford, John Greene, Glenn Ierley, Phil Morrison and Ray Pierrehumbert for many helpful conversations. The 1995 Woods Hole Oceanographic Institution's Summer GFD Program provided a stimulating environment for part of this collaboration. We are grateful to the director, Rick Salmon, and to all the participants for a productive summer. This research was supported by the National Science Foundation under grant OCE 93–01462 and by the UCAR Ocean Modelling Program.

Appendix. Defects in stable, monotonic profiles

In this Appendix we generalize the vorticity defect approximation to more general ambient flow profiles, and include the β-effect. We imagine that the background flow field is described by a profile, $U(y)$, which is stable (to avoid unstable global modes). We then introduce a defect at the level $y = y_0$, and make a Galilean shift into the frame, moving at speed $U(y_0) = U_0$, in which the defect is approximately stationary. Then, the equation of motion for a disturbance takes the form

$$\epsilon\nabla^2\psi_t + (U - U_0)\nabla^2\psi_x + (\beta - U'')\psi_x + \epsilon^2\frac{\partial(\psi, \nabla^2\psi)}{\partial(x, y)} = \epsilon\alpha\left(\epsilon^{-1/2}F - \nabla^2\psi\right) + \epsilon^3\nu\nabla^2\left(\epsilon^{-1}F - \nabla^2\psi\right). \quad \text{(A 1)}$$

Following Stewartson (1978) and Warn & Warn (1978), we pose an outer expansion,

$$\psi = \psi_0 + \epsilon\log\epsilon\psi_{\ell 1} + \epsilon\psi_1 + \ldots. \quad \text{(A 2)}$$

If we introduce this expansion into (A1) and collect the leading-order terms, we find the outer (Fourier-transformed) equation

$$(U - U_0)(\tilde{\psi}_0'' - k^2\tilde{\psi}_0) = (U'' - \beta)\tilde{\psi}_0 \tag{A 3}$$

(i.e. the Rayleigh–Kuo equation). We can solve this equation on either side of the critical layer in order to find two solutions, each of which satisfies one of the boundary conditions at the walls of the channel. We can then match their amplitudes at the critical layer to relate the critical streamfunction amplitude, $\tilde{B}(k,t)$, to the jump in its derivative, $-2\tilde{A}(k,t)$:

$$\tilde{B}(k,t) = \tilde{\mathscr{K}}(k)\tilde{A}(k,t). \tag{A 4}$$

This solution provides a generalized transfer function, analogous to $\mathscr{K}(x - x')$ in (3.9*b*).

A simpler way of finding the outer solution is to turn (A3) into an integral equation (cf. Balmforth & Morrison 1996). We write

$$\tilde{\psi}_0'' - k^2\tilde{\psi}_0 = \mathscr{P}\frac{U'' - \beta}{U - U_0}\tilde{\psi}_0 - 2A\delta(y - y_0), \tag{A 5}$$

and then make use of the Green function, $G_k(y,y')$, of the Laplacian operator on the left-hand side of (A5). Thus, we rewrite (A5) as

$$\tilde{\psi}_0(y) = \mathscr{P}\int_{-1}^{1} G_k(y,y')\left[\frac{U''(y') - \beta}{U(y') - U_0}\right]\tilde{\psi}_0(y')\mathrm{d}y' - 2AG_k(y,y_0). \tag{A 6}$$

This is a singular integral equation that can be regularized by suitably scaling the streamfunction; we let

$$2A = 1 + \mathscr{P}\int_{-1}^{1}\left[\frac{U''(y') - \beta}{U(y') - U_0}\right]\tilde{\psi}_0(y')\mathrm{d}y'. \tag{A 7}$$

Then (A6) becomes

$$\tilde{\psi}_0(y) = \mathscr{P}\int_{-1}^{1}\frac{G_k(y,y') - G_k(y,y_0)}{U(y') - U(y_0)}[U''(y') - \beta]\tilde{\psi}_0(y')\mathrm{d}y' - \Xi G_k(y,y_0), \tag{A 8}$$

which is a regular Fredholm equation of the second kind. This equation is readily solved numerically to furnish the kernel of the transfer function.

As before, we pose an inner expansion of the form (3.10). This leads to the leading-order balance

$$Z_t + U_0'\eta Z_x + (\beta - U_0'')B_x + Z_\eta B_x = \alpha(F - Z) - \nu(F - Z)_{\eta\eta}, \tag{A 9}$$

where $U_0^{(n)} = U^{(n)}(\eta_0)$. We supplement this equation with the integral constraint (3.11) and the transfer relation (3.9*b*). Both the β-effect and the background flow field contribute to a constant vorticity gradient in (A9) (provided it does not vanish, U_0' can simply be scaled out).

At large $|\eta|$, the asymptotic behaviour is governed by

$$U_0'\eta Z_x \sim (U_0'' - \beta)B_x. \tag{A 10}$$

Hence $Z \sim \eta^{-1}$, and so we need to interpret the integral in (3.12) in terms of its principal value. Moreover, the streamfunction behaves like $\eta\log\eta$, which matches the function $\psi_{\ell 1}$ of the outer expansion, (A2), to give a consistent solution.

REFERENCES

Abramowitz, M. & Stegun, I. A. 1972 *Handbook of Mathematical Functions.* Wiley Interscience.

Balmforth, N. J. & Morrison, P. J. 1996 Singular eigenfunctions for shearing fluids. Preprint.

Briggs, R. J., Daugherty, J. D. & Levy, R. H. 1970 Role of Landau damping in crossed–field electron beams and inviscid shear flow. *Phys. Fluids* **13**, 421–432.

Brown, S. & Stewartson, K. 1980 On the algebraic decay of disturbances in a stratified shear flow. *J. Fluid Mech.* **100**, 811–816.

Brunet, G. & Haynes, P. H. 1995 The nonlinear evolution of disturbances to a parabolic jet. *J. Atmos. Sci.* **52**, 464–477.

Brunet, G. & Warn, T. 1990 Rossby wave critical layers on a jet. *J. Atmos. Sci.* **47**, 1173–1178.

Case, K. M. 1960 Stability of inviscid plane Couette flow. *Phys. Fluids* **3**, 143–148.

del-Castillo-Negrete, D., Young, W. R. & Balmforth, N. J. 1995 Vorticity dynamics in shear flow. In *Proc. 1995 Summer Study Program on Geophysical Fluid Dynamics* (ed. R. Salmon). Woods Hole Oceanographic Institution Technical Report.

Davey, A. 1973 On the stability of plane Couette flow to infinitesimal disturbances. *J. Fluid Mech.* **57**, 369–380.

Drazin, P. G. & Howard, L. N. 1966 Hydrodynamic stability of parallel flow of inviscid fluid. *Adv. Appl. Mech.* **9**, 1–89.

Driscoll, C. F. & Fine, K. S. 1990 Experiments on vortex dynamics in pure electron plasmas. *Phys. Fluids* B **2**, 1359–1365.

Gill, A. E. 1965 A mechanism for instability of plane Couette flow and of Poiseuille flow in a pipe. *J. Fluid Mech.* **21**, 503–511.

Haynes, P. H. 1985 Nonlinear instability of a Rossby wave critical layer. *J. Fluid Mech.* **161**, 337–346.

Haynes, P. H. 1987 On the instability of sheared disturbances. *J. Fluid Mech.* **175**, 463–478.

Haynes, P. H. 1989 The effect of barotropic instability on the nonlinear evolution of a Rossby-wave critical layer. *J. Fluid Mech.* **207**, 231–266.

Howard, L. N. 1964 The number of unstable modes in hydrodynamic stability problems. *J. Méc.* **3**, 433–443.

Kelvin, Lord 1887 Rectilinear motion of fluid between two parallel plates. *Phil. Mag.* **24**, 188–196.

Killworth, P. & McIntyre, M. 1985 Do Rossby wave critical layers absorb, reflect or overreflect? *J. Fluid Mech.* **161**, 449–492

Landau, L. 1946 On the vibration of the electronic plasma. *J. Phys. USSR* (*Moscow*) **10**, 85–93.

Lerner, J. & Knobloch, E. 1988 The long–wave instability of a defect in a uniform parallel shear. *J. Fluid Mech.* **189**, 117–134.

Maslowe, S. A. 1985 Shear flow instabilities and transition. In *Hydrodynamic Instabilities and the Transition to Turbulence*, 2nd Edn (eds. H. L. Swinney & J. P. Gollub). Springer.

Murdock, J. W. & Stewartson, K. 1977 Spectra of the Orr–Sommerfeld equation. *Phys. Fluids* **20**, 1404–1411.

Nicholson, D. R. 1983 *Introduction to Plasma Theory*. Wiley.

Orr, W. McF. 1907 Stability or instability of steady motions of a perfect fluid. *Proc. R. Irish Acad.* **27**, 6–69.

Penrose, O. 1960 Electrostatic instabilities of a uniform non-Maxwellian plasma. *Phys. Fluids* **3**, 258–265.

Pillai, S. N. & Gould, R. W. 1994 Damping and trapping in 2D inviscid fluids. *Phys. Rev. Lett.* **73**, 2849–2852.

Pipkin, A. C. 1991 *A Course on Integral Equations.* Springer.

Rosenbluth, M. N. & Simon, A. 1964 Necessary and sufficient condition for the stability of plane parallel inviscid flow. *Phys. Fluids* **7**, 557–558.

Schmid, P. J., Henningson, D. S., Khorrami, M. R. & Malik, M. R. 1993 A study of eigenvalue sensitivity for hydrodynamic stability operators. *Theor. Comput. Fluid Dyn.* **4**, 227–240.

Stewartson, K. 1978. The evolution of the critical layer of a Rossby wave. *Geophys. Astrophys. Fluid Dyn.* **9**, 185–200.

Warn, T. & Warn, H. 1978. The evolution of a nonlinear critical level. *Stud. Appl. Maths* **59**, 37–71.

Weitzner, H. 1963 Plasma oscillations and Landau damping. *Phys. Fluids* **6**, 1123–1127.